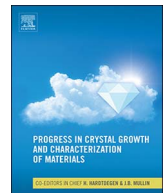




Contents lists available at ScienceDirect

# Progress in Crystal Growth and Characterization of Materials

journal homepage: [www.elsevier.com/locate/pcrysgrow](http://www.elsevier.com/locate/pcrysgrow)

## Epitaxial growth of highly mismatched III-V materials on (001) silicon for electronics and optoelectronics

Qiang Li<sup>a,b,\*</sup>, Kei May Lau<sup>a,b</sup><sup>a</sup> Department of Electronic and Computer Engineering, Hong Kong University of Science and Technology, Clear Water Bay, Kowloon, Hong Kong<sup>b</sup> Institute for Advanced Study, Hong Kong University of Science and Technology, Clear Water Bay, Kowloon, Hong Kong

### A B S T R A C T

Monolithic integration of III-V on silicon has been a scientifically appealing concept for decades. Notable progress has recently been made in this research area, fueled by significant interests of the electronics industry in high-mobility channel transistors and the booming development of silicon photonics technology. In this review article, we outline the fundamental roadblocks for the epitaxial growth of highly mismatched III-V materials, including arsenides, phosphides, and antimonides, on (001) oriented silicon substrates. Advances in heteroepitaxy and selective-area hetero-epitaxy from micro to nano length scales are discussed. Opportunities in emerging electronics and integrated photonics are also presented.

### 1. Introduction

Mismatched hetero-epitaxy of semiconducting materials allows for tailoring of heterojunctions, strain manipulation, and device integration for a wide range of applications. One exemplary topic of study is the growth of cubic III-V semiconductors on lattice-mismatched (001) Si substrates. Si is the backbone material in digital integrated circuits for logics and signal processing. It possesses some attractive properties, like larger wafer size, better thermal conductivity, low-cost and mature manufacturing, and natural-abundance. III-V semiconductors, by contrast, have their niches in applications from optoelectronics to high-frequency and high-speed devices, for their superior electron mobilities and direct bandgap properties. The concept of monolithic III-V/Si integration began as a simple notion, that the best features and utility of III-V materials and devices could be combined with the benefits of Si manufacturing [1]. Despite the tremendous effort put into this field, progress had been slow until this topic regained momentum a few years ago, driven by the development of emerging transistors [2] and Si photonics technology [3].

The purpose of this review article is to update recent advances in the epitaxial growth of large lattice-mismatched III-V materials on (001) Si substrates. Nearly lattice-matched hetero-epitaxy (e.g., GaP on Si [4–6]) or pseudomorphic growth [7,8] is important but will not be discussed here. We focus on the growth performed on (001) oriented Si, rather than those on (111) Si (e.g., the vapor-liquid-solid growth method), for compatibility with the mainstream complementary-metal-oxide-semiconductor (CMOS) technology. Both wafer-level hetero-

epitaxial thin film growth and selective-area hetero-epitaxy will be presented. Their respective device applications are discussed in detail.

### 2. Fundamental challenges in III-V hetero-epitaxy on (001) silicon

Growing fully relaxed, lattice-mismatched materials on a foreign substrate is often referred to as “metamorphic growth” [9]. There are several fundamental challenges that limit the quality of metamorphic III-V layers on (001) Si, including a large mismatch in the lattice constants and thermal expansion coefficients, as well as the growth of polar materials on non-polar substrates. Fig. 1 plots the bandgap energy/wavelength versus lattice constant/misfit for group III-V and group-IV materials. In III-V/Si hetero-epitaxy, the introduction of dislocations is necessary to accommodate the structural mismatch. For arsenides and phosphides material systems, films grown past the pseudomorphic critical thickness generally relax through the nucleation of dislocation half loops at the surface, which glide down on the {111} plane towards the hetero-interface, creating 60° misfits and threading dislocations in the process. These threading dislocations, with a density up to  $10^9\text{--}10^{10}/\text{cm}^2$ , act as non-radiative recombination and carrier scattering centers, change local strain, and lead to device early failures. Achieving a low threading dislocation density (TDD) is therefore one of the most important metrics for metamorphic epitaxial growth. The thermal expansion mismatch limits the maximum buffer thickness that can be used. Macroscopic cracks emerge if a thick buffer accumulates too much strain energy upon temperature changes. With linear thermal expansion coefficients of Si, GaAs, and InP being  $2.59 \times 10^{-6}/\text{K}$ ,

\* Corresponding author.

E-mail address: [eeqli@ust.hk](mailto:eeqli@ust.hk) (Q. Li).

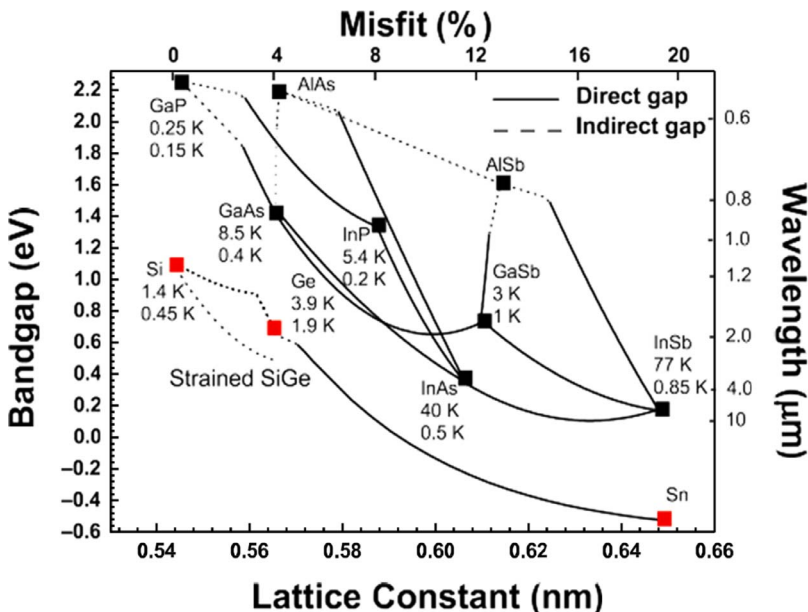


**Fig. 1.** Plot of bandgap energy/wavelength versus lattice constant/misfit for III-V, Si/Ge/Sn. The numbers below the chemical symbols are electron and hole mobilities in units of  $\text{cm}^2/\text{Vs}$ . The solid lines indicate direct bandgaps. (The red symbols are column IV elements.) [10]. (For interpretation of the references to colour in this figure legend, the reader is referred to the web version of this article.)

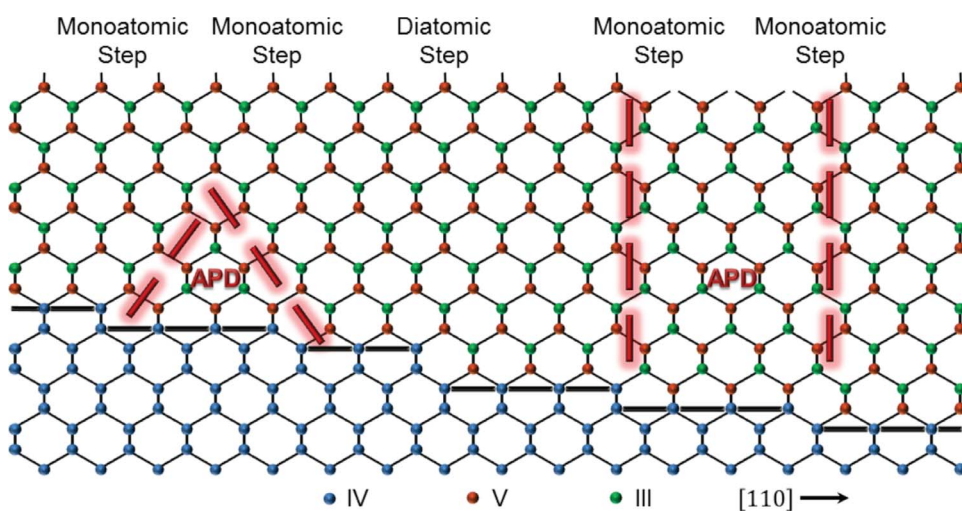


**Fig. 2.** Schematic down  $[1\bar{1}0]$ , showing non-polar/polar interface between the group IV substrate and III-V epilayer. Monoatomic steps on the group IV substrate surface result in APBs, which are planes of V-V or III-III bonds. The APD can either self-annihilate (left) or rise to the surface (right). Diatomic steps on the substrate surface (center) do not result in APD formation. [27].

$5.73 \times 10^{-6} / \text{K}$ , and  $4.6 \times 10^{-6} / \text{K}$  respectively, the thickness of heteroepitaxial III-V thin films on Si is typically limited to about  $10 \mu\text{m}$  and below [11,12]. Experimentally observed critical thickness for the onset of crack formation in GaAs epilayers on Si is approximately  $7 \mu\text{m}$  for a  $\Delta T$  of  $575^\circ \text{C}$ ,  $5.1 \mu\text{m}$  for a  $\Delta T$  of  $675^\circ \text{C}$ , and  $4.9 \mu\text{m}$  for a  $\Delta T$  of  $725^\circ \text{C}$  [13], where  $\Delta T$  represents the change in temperature in the cooling-down stage after growth.

It is interesting to note exceptions in III-Sb on GaAs and III-Sb on Si hetero-epitaxy. With the extremely large lattice mismatch and the softness nature of antimoniides, strain relaxation can occur by the formation of  $90^\circ$  pure edge-type misfit dislocations (MDs) [14–17]. These sessile MDs, arranged in a two-dimensional (2D) network and confined at the hetero-interfaces, provide the most efficient strain relaxation and do not easily thread upward into the layers grown atop. This fundamentally different growth mode is referred to as the interfacial misfit (IMF) growth mode. High quality GaSb thin films have been reported without resorting to several- $\mu\text{m}$ -thick metamorphic buffer layers [18]. The prevailing approach to perform IMF growth of III-Sb on Si is to begin with an ultra-thin AlSb nucleation layer [19–21], such that a periodic array of  $90^\circ$  misfit dislocations, akin to those in the IMF growth of GaSb on GaAs, can be created. Apart from the advantages of the IMF growth mode, the thermal expansion coefficient of AlSb ( $2.55 \times 10^{-6} / \text{K}$ ,

$K$  at  $300 \text{ K}$ ) is very close to that of Si ( $2.59 \times 10^{-6} / \text{K}$  at  $300 \text{ K}$ ). With a relatively small thermal expansion coefficient mismatch, absence of microcracks or wafer bending even in very thick ( $10 \mu\text{m}$ ) AlSb on a Si wafer has been reported [22]. In the past few years, III-Sb-based quantum-well edge-emitting laser diodes monolithically grown on Si substrate have been demonstrated [23–25], covering wavelengths from near  $2 \mu\text{m}$  to  $1.5 \mu\text{m}$  telecom wavelength range.

A unique type of defect associated with III-V/Si hetero-epitaxy is antiphase-domains (APDs), which arise from the lack of inversion symmetry of III-V materials. As a group IV semiconductor, Si crystallizes in a diamond structure, with two face-centered-cubic (FCC) sublattices occupied by the same type of atom species. Each Si atom is bonded to four neighboring Si atoms in a tetrahedral arrangement, and the bonding electrons are shared equally between the nuclei. As a result, Si is a non-polar material. In contrast, for cubic III-V semiconductors with a zinc-blende crystal structure, the two FCC sublattices are occupied by different atom species. The bonds are polar due to the difference in the ionicity of the constituent atoms. The cubic zinc-blende structure's symmetry forbids spontaneous polarization but allows piezoelectric polarization [26].

APDs are inherent to polar-on-non-polar growth. In practice, any real (001) Si surface always exhibits steps. Single-layer steps (or odd

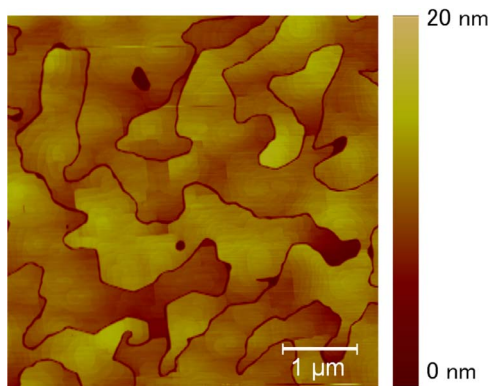


**Fig. 3.** AFM image of as-grown GaAs on an exact (001) Si substrate by MOCVD, showing APBs appearing in irregular shapes.

layer height steps) produce two domains in the III-V overlayer with opposite sublattice allocation (see Fig. 2 [27]), whereas double-layer (or even-numbered) steps do not. The two III-V domains are separated by a plane of wrong bonds, either III-III or V-V bonds, which is referred to as an antiphase boundary (APB) or inversion domain boundary (IDB). APBs are electrically charged planar defects, acting as non-radiative recombination centers in optoelectronic devices and leakage paths in electronic devices. The impact of APBs on the optical properties of III-V layers is often characterized by photoluminescence quenching and spectral broadening [28,29], while their role on electrical properties is reflected in the significantly degraded electron mobilities [29,30]. With certain growth or etching conditions, APBs rising to the material surface could be visible under scanning electron microscopy (SEM) or atomic force microscopy (AFM). As an example, Fig. 3 displays an AFM image of as-grown GaAs on an exact (001) Si substrate by metal-organic chemical vapor deposition (MOCVD), showing irregular, curved boundaries.

Another fundamental problem originating from growing a polar semiconductor on a non-polar substrate is the lack of charge neutrality [31,32] at the III-V/Si interface, and the related interdiffusion leading to cross-doping of both materials. In GaAs/Si heteroepitaxy, as As forms strong bonds with Si, whereas Ga does not, the first atomic layer bonding to the Si substrate will be an As layer. Without atomic re-arrangement, the As-Si bonds would carry a charge density equivalent to  $3 \times 10^{14}$  donors/cm<sup>2</sup> and support a huge electric field of about  $3 \times 10^{14}$  V/cm inside the growing GaAs layer [31]. Such a large field can lead to massive atomic re-arrangements, attempting to restore a neutral interface. Harrison et al. [32] have considered two idealized atomic arrangements, both of which involving a fraction of Si atoms being replaced by Ga atoms and re-incorporated into the first As plane. Under realistic finite-rate growth conditions, the Si atoms that are removed from the top Si layer have a good chance to be simply taken up by the growing GaAs as bulk dopant. As a consequence, the accumulated Si atom on the GaAs surface can easily diffuse across the heterointerface during high temperature annealing. Moreover, experimental observations revealed a significant enhancement of the Si diffusivity in the presence of a high level of crystalline disorder at the heterointerface [33]. This is even more severe in GaAs-Ge-Si structures. The outdiffusion of Si and Ge into the III-V layer implies a need for diffusion barrier layer to prevent large leakage current that makes device operation untenable [34].

### 3. Wafer-scale hetero-epitaxial growth of III-V thin films on Si

Since the 1980s, tremendous effort has been applied to the epitaxial growth of device-quality III-V thin films on lattice-mismatched Si wafers, mostly by MOCVD or molecular beam epitaxy (MBE). GaAs-on-Si has been the most heavily investigated since the problems associated

with GaAs/Si hetero-epitaxy are representative of the difficulties associated with the growth of lattice-mismatched and polar-on-non-polar semiconductor hetero-structures [35]. The insight gained from studying this material could aid the conception and optimization of other hetero-epitaxial systems. The APB problem has been fairly successfully resolved by the use of misoriented Si substrates in conjunction with high-temperature pre-bake treatment [36–38]. Beginning with a 4–6° offcut Si substrate tilted toward the [110] direction, single atomic steps tend to reorganize into energetically more stable double steps under high-temperature annealing conditions [39]. As a result, the APB can be minimized or eliminated. In direct GaAs-on-Si epitaxy with an abrupt transition from the substrate to the overgrown GaAs, a two-step method [30] is widely adopted to improve the structural perfection of the hetero-epitaxial thin films. Post-growth thermal cycle annealing [40–42], by which an epilayer is subjected to large temperature oscillations and thus periodically switching between compressed and tensile states [43], has been found effective in reducing threading dislocation densities. Insertion of dislocation filter layers, such as a strained layer superlattice [44] or thin strained layers [45], can facilitate the annihilation of threading dislocations thereby minimize intrusion of dislocations in the active layers of interest. Growth of compositionally graded buffers (e.g., SiGe, GaAsP) [46–48] to bridge the lattice constant between Si and GaAs is another approach that has been heavily investigated. Achieving high strain relaxation while maintaining a low threading dislocation density are figures of merit of such metamorphic graded buffers. Over the past three decades, the above-mentioned techniques, often combined together, have been used to grow various compound semiconductors on Si, leading to different levels of success. The reader is referred to several previous reviews [35,49] for more comprehensive discussions.

More recently, some major advancements have been made in blanket hetero-epitaxy of III-V compound semiconductors on planar Si substrates, including scaling III-V integration up to 300-mm Si wafers, overcoming the APD problem on exact (001) oriented Si, and demonstrating high-mobility quantum-well (QW) transistors and low-threshold quantum-dot (QD) lasers.

The diameter of III-V substrates is often limited to 150 mm or less, while the maximum Si wafer diameter is 300 mm commercially, with 450 mm in development. Scaling III-V integration up to 300 mm Si to make use of state-of-the-art Si manufacturing foundries provides cost advantages. In the past few years, direct growth of III-V materials of interest on 200 mm and 300 mm Si wafers has been reported by a number of groups. Roesener et al. [50] proposed and investigated the growth of GaP nucleation and metamorphic  $\text{Ga}_x\text{In}_{1-x}\text{P}$  buffers on 300 mm Si for solar cell integration. Today, 300 mm GaP/Si templates (NASP<sub>III/V</sub> GmbH [51]) grown by MOCVD are commercially available. Recent GaAsP metamorphic solar cells [52,53] epitaxially grown on GaP/Si substrates have demonstrated efficiencies above 11.5% by reducing the TDD values down to  $4.0\text{--}4.6 \times 10^6 \text{ cm}^{-2}$ , showing a promising path towards high-efficiency dual-junction GaAsP-on-Si cells. Motivated by the development of III-V channel MOSFETs for high-performance and low-power logic applications, Huang et al. [54] and Orzali et al. [55] reported epitaxy of smooth  $\text{In}_{0.53}\text{Ga}_{0.47}\text{As}$  layers on 300 mm Si wafers using metamorphic InP/GaAs buffers by MOCVD. The GaAs/InP metamorphic buffer was reduced to  $\sim 860 \text{ nm}$  in thickness, among the thinnest in the literature. By defect counting or Ayers' model [56], TDD in the low  $10^9 \text{ cm}^{-2}$  range was determined.

Having of III-V/Si epitaxy on 300 mm substrates also presents opportunities to overcome wafer size incompatibility in wafer bonding technology. By growing III-V layers on a Si donor wafer instead of on a lattice-matched III-V native donor wafer, III-V-on-insulator-on-Si substrates with any available wafer size can be realized [57,58]. Proof-of-principle demonstrations of 100 mm InGaAs-on-insulator [59] and 200 mm InGaAs-on-insulator wafers [60,61] were first reported. In the fabrication process flow described in Fig. 4,  $\text{In}_{0.53}\text{Ga}_{0.47}\text{As}$  was directly grown by MBE on a 200 mm Si substrate. A  $2.5 \mu\text{m}$  Ge buffer, followed

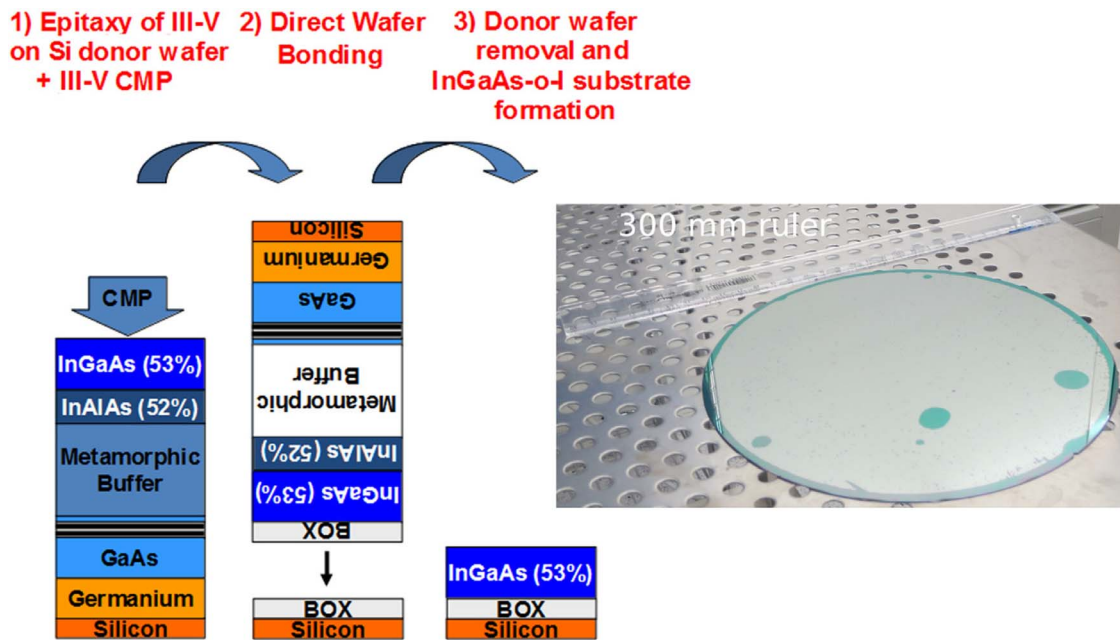


**Fig. 4.** The fabrication process flow consists of doing the chemical mechanical polishing (CMP) directly on InGaAs and depositing an ultrathin buried oxide (BOX) prior to the direct wafer bonding (DWB) and transfer. A picture of a 200 mm InGaAs-on-insulator is shown [60].

by 0.5 µm Ga(Al)As and 1.5–2 µm  $In_xAl_{1-x}As$  metamorphic buffer, was grown to accommodate the lattice mismatch between InGaAs and Si. The wafer was then planarized using chemical mechanical polishing (CMP). An ultrathin  $Al_2O_3$  buried oxide (BOX) layer was deposited for direct wafer bonding. The donor wafer was subsequently removed by wet-etching, leaving a 200 mm InGaAs-on-insulator substrate. Very recently, a similar process but improved to allow donor wafer recycling was developed, leading to successful fabrication of 300 mm InGaAs-on-insulator substrates [62]. These processes open the way to very large-scale production of III-V-on-insulator hybrid substrates for future technology nodes. However, a major limitation still lies in the high density of crystal defects generated in blanket hetero-epitaxy on the donor Si substrates.

For III-V/Si integration to be compatible with CMOS processing and devices, microelectronics-standard nominal (001) Si substrates with a miscut angle less than 0.5° are preferred [5]. However, except for nearly lattice-matched GaP on Si [5], conventional hetero-epitaxy on planar Si wafers generally requires a 4°–6° offcut angle in order to form a prominent double-stepped Si surface that prevents APDs. Recently, there has been notable progress made to achieve APB-free III-V epitaxial layers on the so-called “exact” Si (001) substrates by careful treating of

(001) Si with a slight misorientation (< 0.5°) prior to III-V nucleation [29]. Fig. 5(a) shows an AFM image of a 400 nm thick GaAs layer grown on un-optimized on-axis Si (001) substrates, showing a high density of randomly oriented APBs. In Fig. 5(b), a quasi Si (001) substrate with a 0.15° misorientation in the [110] direction is deoxidized in a SiCon™ chamber using  $NF_3/NH_3$  remote plasma and then annealed (1 min–10 min) in an MOCVD reactor at high temperature (800 °C–950 °C) in  $H_2$  ambient. Such a surface preparation procedure promotes the structuring of the 2 × 1 surface and forms predominant double steps, as shown in Fig. 5(b). This observation appears to contradict theoretical thermodynamics, which suggests it is energetically unfavorable to form a double-stepped Si surface at a low miscut angle. Bruckner et al. [63] attributed this anomalous phenomenon to the interaction of the Si surface with the  $H_2$  ambient driving a dynamic step formation process governed by surface vacancy generation, diffusion, and annihilation at the step edges. With the double-stepped Si in Fig. 5(b), subsequent growth of a 150 nm GaAs overlayer shows APB-free surface, as shown in Fig. 5(c). These results coincide with the experimental observation from a number of groups that single-domain Ge and III-V layers can be deposited on nominal Si (001) substrates [54,55,64–67].

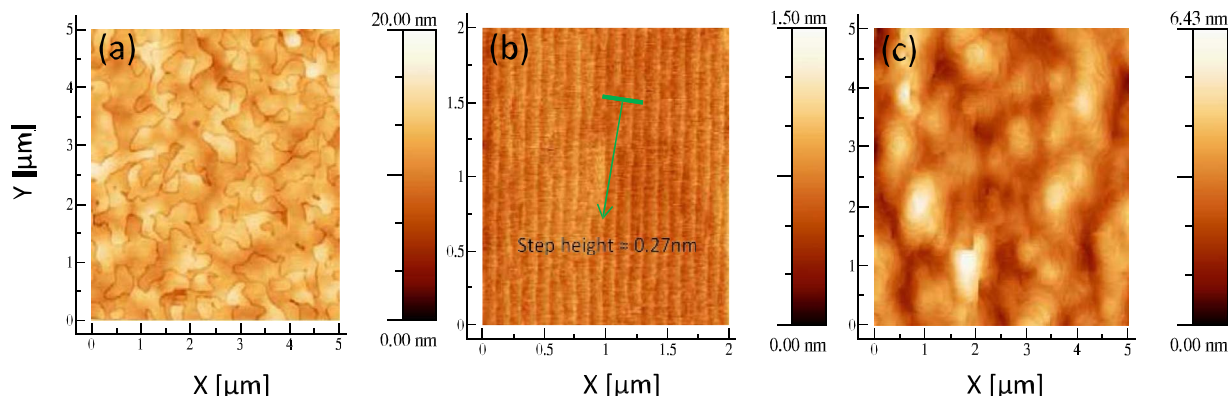


**Fig. 5.** (a) 5 × 5 µm<sup>2</sup> AFM image of 400 nm thick GaAs growth on un-optimized Si(001): High density of randomly oriented APBs; RMS roughness = 1.6 nm. (b) 2 × 2 µm<sup>2</sup> AFM image of 0.15° Si (001) after optimized preparation (800 °C–950 °C annealing under  $H_2$ ). The surface is therefore mainly double-stepped. (c) 5 × 5 µm<sup>2</sup> AFM image of APBs-free 150 nm thick GaAs growth on optimized 0.15° Si(001); RMS roughness = 0.8 nm. [29].

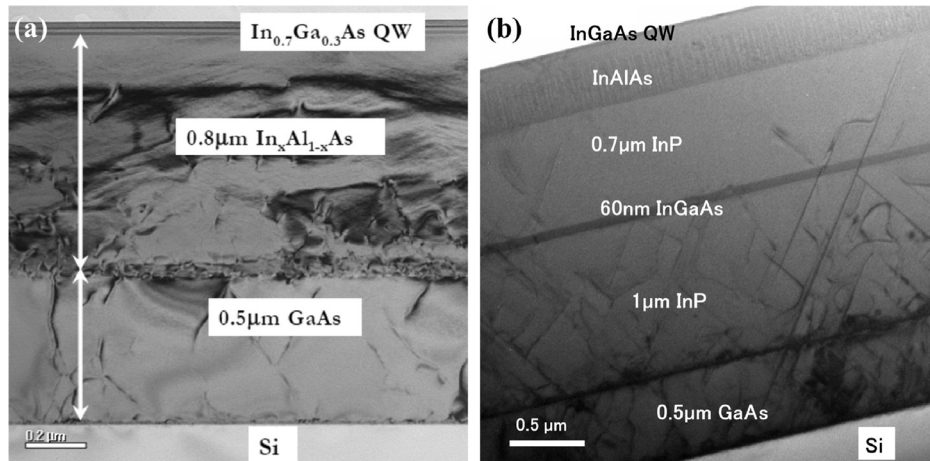


**Fig. 6.** Cross-sectional TEM image of InGaAs quantum-well field-effect transistor structures on Si using compositionally graded InAlAs/GaAs buffer by MBE (a) [69] and InP/GaAs buffer by MOCVD (b) [66].

The last few years have witnessed a booming development in heterogeneous integration of III-V transistors and light emitters on Si. High-mobility III-V semiconductors, such as InGaAs/InP- and GaSb/InAs-based materials, are of great interest for digital logic device applications due to their potential to replace Si channel in emerging MOSFETs and their potential for developing innovative device structures like tunnel FETs [2,68]. Both MBE and MOCVD have demonstrated excellent InGaAs QW heterostructures on (001) Si substrates [64,66,69,70], with room-temperature Hall mobilities exceeding 10,000 cm<sup>2</sup>/V·s, matching the best results on native InP substrates. In these metamorphic device structures, compositionally graded InAlAs/GaAs or composite InP/GaAs buffers, a few micrometers thick, have been used to convert the lattice constant of Si to the desired one in the active layers, as shown by the cross-sectional transmission electron microscopy (TEM) images in Fig. 6. Different transistor structures, including QW field-effect transistors with Schottky gates [69,71], and QW channel MOSFETs with high-k dielectrics [70] and source/drain regrowth [72–76], have been reported. These exploratory transistors demonstrated record-high drive current and extrinsic transconductance at low operation voltages, suggesting potential for high-speed switching applications with reduced power consumption. Challenges remain, however, in their compatibility with CMOS processing, integration with p-channel transistors, and device uniformity and reliability issues arising from surface roughness and high dislocation density.

Integration of III-V lasers on Si has been under investigation for some time. More recent interest has been motivated by the fast-evolving Si photonics technology. Si is a good waveguiding material but poor in light emission. Despite progress in Si-based light modulation and detection technology, and low-cost Si optoelectronic integrated devices enabled by the mature CMOS technology [77,78], an efficient, reliable

laser on a Si substrate remains the “holy grail” for Si photonics. Heterogeneous integration of III-V materials on silicon combines the superior gain characteristics of compound semiconductors with the passive waveguide characteristics of Si. Among various integration schemes, hybrid III-V-on-Si laser through wafer bonding technology is considered the most successful and being commercialized [79]. There have been many significant advances in device performance [80–85] using improved fabrication technologies compatible with silicon photonics. However, epitaxial growth of III-V lasers on Si is ultimately preferred as a monolithic and sustainable integration solution. Compared to the bonding approaches, it offers a scalable process which is desirable for large-scale commercial applications. Cost advantages follow as well when process integration schemes are well-defined.

Attempts to grow III-V QW lasers directly on Si date back to the 1980 s. In 1987, room-temperature continuous-wave (CW) operation of large-area GaAs/AlGaAs hetero-structure lasers on (100) Si substrates was obtained [86]. The laser operated on four different occasions for a total of 4 min before degradation took place. In 1991, room-temperature CW operation of an InGaAs/InGaAsP multi-quantum-well (MQW) laser diode on a Si substrate was reported [87], and in 2003, GaAs/AlGaAs QW lasers were demonstrated on relaxed graded Ge/GeSi virtual substrates on Si [88]. In general, most of previous QW lasers on Si suffered from poor reliability and short lifetimes, impeding their practical application. The rapid degradation was attributed to the formation of dark line defects [89–95]. Fig. 7 illustrates the growth of a dislocation network in the active layer of a laser device. (a) Initially, the dislocation PN with the Burgers vector  $b$  crosses the layer; then (b) climbs into the active zone; (c) further climbing confined to the active zone causes elongation along the [100] direction [89].

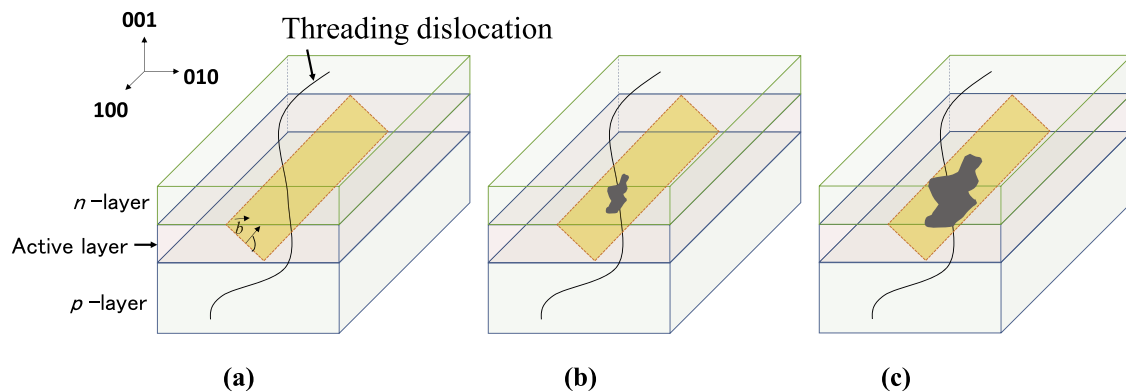


**Fig. 7.** Scheme of the growth of a dislocation network in the active layer of a laser device. (a) Initially, the dislocation PN with the Burgers vector  $b$  crosses the layer; then (b) climbs into the active zone; (c) further climbing confined to the active zone causes elongation along the [100] direction [89].

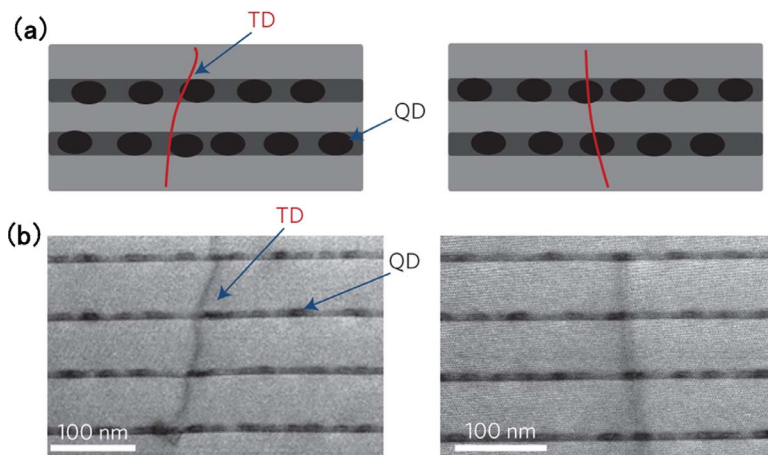


**Fig. 8.** (a) Schematic of the interaction between QDs and threading dislocations. (b) Bright-field scanning TEM images showing the potential interactions between threading dislocations and QDs [99].

mechanism of III-V lasers and light emitting diodes. As a consequence, the achievement of a GaAs- or InP-based QW laser on Si that can simultaneously exhibit low threshold current, high temperature stability, and long lifetime has remained elusive [97]. To overcome this fundamental challenge, recent implementation of compound semiconductor lasers on Si has been focused on using QDs as the gain material. Because of their inherent property of carrier confinement/localization and reduced interaction with defects, QDs have proved to be less sensitive to defects than conventional bulk materials and QW structures [97–99]. As shown in Fig. 8, a threading dislocation can only ‘kill’ a very limited number of QDs, leaving the rest intact and able to provide optical gain. Moreover, the strong strain field of a QD array can bend the propagation of threading dislocations [97] or propel threading dislocations away from the QDs [99]. For these reasons, III-V QD lasers grown on Si could potentially deliver superior reliability with relaxed tolerance to TDD. Pioneering work on self-organized  $In_{0.5}Ga_{0.5}As$  QD lasers on Si incorporated multiple stacked InAs QD layers in the buffer as effective dislocation filters [97,100]. These QD lasers, with an emission wavelength close to 1  $\mu\text{m}$ , exhibited relatively low threshold current (900  $\text{A}/\text{cm}^2$ ) and very high characteristic temperature ( $T_0 = 278 \text{ K}$ ).

Significant progress has been made ever since to achieve room-temperature CW lasing at the telecommunication band of 1.3  $\mu\text{m}$ . The first operation of InAs QD lasers epitaxially grown on a Ge substrate was demonstrated in 2011 [101]. Using a Ga prelayer growth technique, an APB-free GaAs buffer layer was grown on offcut Ge substrates by MBE. Broad-area laser devices with a five-layer InAs/InGaAs dot-in-a-well (DWELL) active structure were fabricated, realizing room-temperature CW lasing at 1305 nm with an output power of  $\sim 28 \text{ mW}$  per facet and a very low threshold current density of  $55.2 \text{ A cm}^{-2}$ . Since Ge is widely used as the transitional buffer for GaAs-on-Si hetero-epitaxy, this result marks an important milestone in the monolithic integration of long-wavelength InAs/GaAs QD lasers on a Ge/Si substrate. Leveraging the well-established Ge-on-Si epitaxy technique, Liu et al. [102] were able to fabricate 1.3  $\mu\text{m}$  InAs QD ridge lasers more in line with commercial telecom laser designs. Room-temperature low thresholds (16 mA), high output power (176 mW), high-temperature lasing (up to 119 °C), and high  $T_0$  ( $> 200 \text{ K}$ ) were reported. The device yield measurements showed repeatable performance across different dies and wafers. Reliability tests uncovered over 2700 h of continuous wave operation at 30 °C along with an extrapolated mean time to failures of up to 4600 h [103]. This remarkable progress suggests great potential for producing reliable and efficient QD lasers on Si by further increasing the ratio of lasing QDs to dislocations.

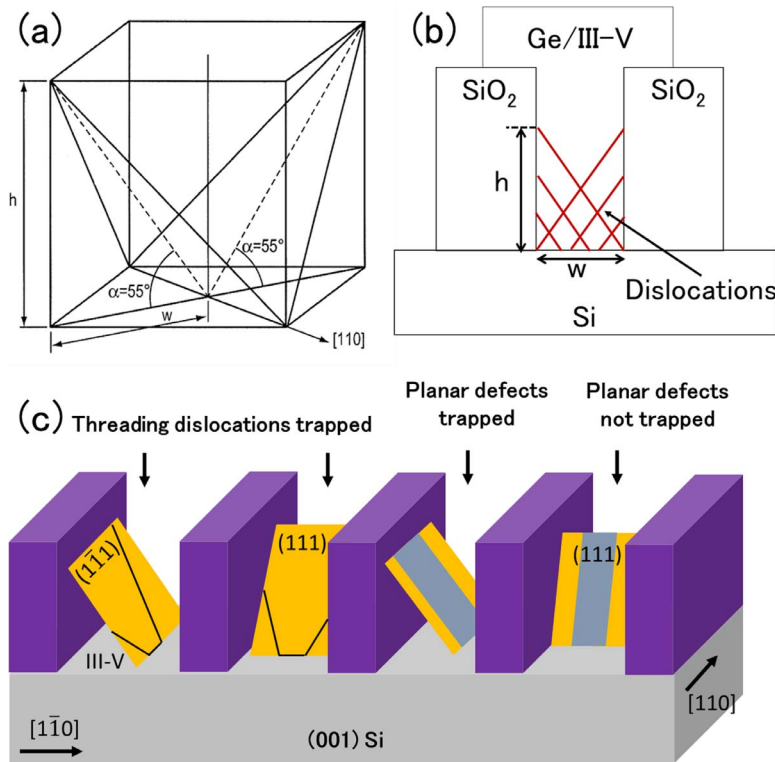
The results of high-performance QD lasers on both Ge-on-Si and Ge substrates are encouraging. However, it would be more attractive to realize a laser that does not require an intermediate Ge layer, both because the requirement of the Ge layer restricts the range of Si circuits to which it can be applied and because it is difficult to couple light

through this layer to a Si waveguide due to the large optical absorption coefficient of Ge at telecommunications wavelengths [99]. Combining a thin nucleation layer made of AlAs, a multi-temperature growth method and InGaAs/GaAs superlattices filters, Chen et al. [99] reported InAs/GaAs QD lasers directly grown on Si substrates with a record-low threshold current density of  $62.5 \text{ cm}^{-2}$ . Broad-area lasers were fabricated with as-cleaved facets, realizing CW lasing up to 75 °C, a high output power exceeding 105 mW at room temperature, and a long extrapolated lifetime of over 100,158 h. In all the above-mentioned QD lasers on Si, offcut Si (001) substrates were used to suppress the anti-phase disorder arising from the polar-on-non-polar hetero-epitaxy.

Most recently, extensive research has been performed on quantum dot lasers monolithically grown on “exact” (001) Si substrates that are standard in microelectronics fabrication. Leveraging an APB-free GaP-on-Si (001) template, Liu et al. [104] demonstrated the first electrically pumped CW InAs QD lasers epitaxially grown on (001) Si without offcut. By growing APB-free GaAs thin films on V-groove patterned (001) Si, Norman et al. [105] reported electrically injected, Fabry-Perot QD ridge lasers, showing CW operation up to 80 °C with threshold currents as low as 37 mA. Chen et al. [106] reported electrically pumped 1.3  $\mu\text{m}$  InAs/GaAs QD lasers directly grown on microelectronics-standard planar (001) Si substrates using a sophisticated Si surface preparation step. These results demonstrate the compatibility of high-performance monolithic III-V light sources with on-axis Si substrates and their potential for CMOS foundry integration.

#### 4. Selective-area hetero-epitaxy from micrometer to nanometer length scale

Selective-area hetero-epitaxy, which restricts epitaxial growth in pre-defined regions by substrate patterning, offers additional control over the strain relaxation process and brings benefits like the defect necking effect. Over the past few decades, selective-area hetero-epitaxy has been extensively investigated in Ge/Si and III-V/Si material systems, spanning the micro- to nanoscales. One unique growth method derived from selective hetero-epitaxy is referred to the “aspect ratio trapping” (ART) technique. By this approach, III-V materials are selectively grown in high-aspect-ratio holes or trenches formed by a patterned dielectric (typically  $\text{SiO}_2$ ) on Si. The threading dislocations originating from the III-V/Si hetero-interface are guided to the oxide sidewalls should the aspect ratio allow, resulting in dislocation-free regions above a critical thickness. The “trapping” of threading segments (i.e., the epitaxial necking effect) in the ART technique is attributed to the inherent crystallographic geometry. In the  $\{111\}/<110>$  cubic slip system, misfit dislocations lie along the  $\langle 110 \rangle$  directions in the (100) growth plane, while the threading segments rise up on the  $\{111\}$  planes in the  $\langle 110 \rangle$  directions [107]. As shown in Fig. 9(a), for an  $[110]$  direction aligned trench with a trench width of  $w$  and an oxide sidewall



height of  $h$ ,  $<110>$ -oriented threading segments would all be inclined to the  $[1\bar{1}0]$  oxide sidewalls, and their projections onto the  $(110)$  plane would form a  $\sim 55^\circ$  angle with the  $[1\bar{1}0]$  direction. In principle, when the aspect ratio ( $AR = h/w$ ) is larger than 1.4, all the threading dislocations will project into the oxide wall and terminate there. This also implies an interesting fact, that if the trenches/holes are small enough, the dislocation elimination can be accomplished within a very thin buffer layer, preventing stress accumulation caused by the thermal expansion coefficient mismatch. The ART concept (see Fig. 9(b)) was firstly revealed in Ge/Si hetero-epitaxy [108], and then applied to III-V/Si epitaxy. The trapping capability of the ART structure for dislocations and planar defects is further explained schematically in Fig. 9(c). For  $60^\circ$  threading dislocations generated during growth, they tend to glide along the  $\langle 111 \rangle$  planes. These dislocations will eventually hit an oxide wall if the trench aspect ratio is sufficiently high. In the same way, planar defects on  $\{111\}$  planes parallel to the trenches are trapped. Only planar defects lying in planes perpendicular to the trenches will never be blocked [109]. Experimental studies show that those dislocations in selective hetero-epitaxy can undergo significant redirection, so as to follow the normal to the newly formed crystal facets as growth proceeds [107], but the defect trapping effect still holds.

Fig. 10(a) displays a tilted-view SEM image of GaAs selectively grown on a sub-micron-stripe-patterned  $(001)$  Si substrate by MOCVD. We can observe  $(111)$  GaAs faceting at the growth front with an excellent growth uniformity. In Fig. 10(b), the propagation of crystalline defects revealed by cross-sectional annular dark field scanning transmission electron microscopy (STEM) agrees well with the ART concept, although the dielectric stripes are not tall enough to provide a sufficiently large aspect ratio for complete defect necking. Development of the ART growth of III-V materials on Si has gone from micro- to nano-scale lengths [110–113]. In Fig. 11(a), the aspect ratio of the trenches is large enough so that all the dislocations are essentially trapped under the dash line. However, hard-to-control asymmetry of GaAs facets remains a problem. It should be noted that the top facets of GaAs can be manipulated by growth conditions. Fig. 11(b) shows a flat GaAs(001) top surface which is considered more amenable for device fabrication

**Fig. 9.** (a) Schematic showing the crystallography of mismatch relaxation-related glissile threading dislocations and their projections onto the  $(110)$  plane ( $w$  is the width of the trench, while  $h$  is the height of the sidewall) [107]. (b) Cross-section diagram demonstrating the principles of epitaxial necking, showing zero threading dislocations at the upper surface [108]. (c) The trapping capability of the ART technique for threading dislocations and planar defects [109].

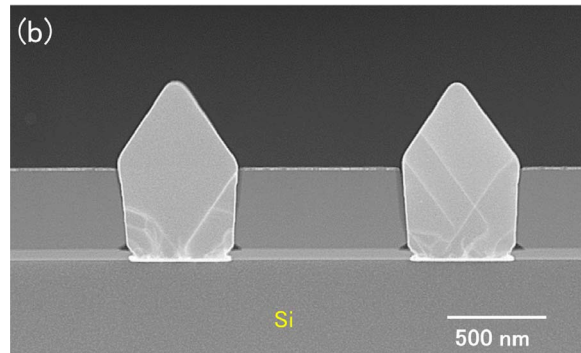
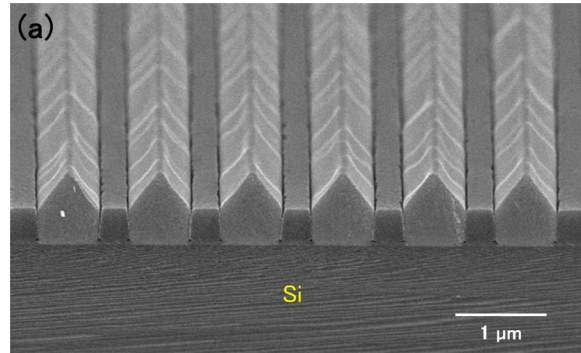
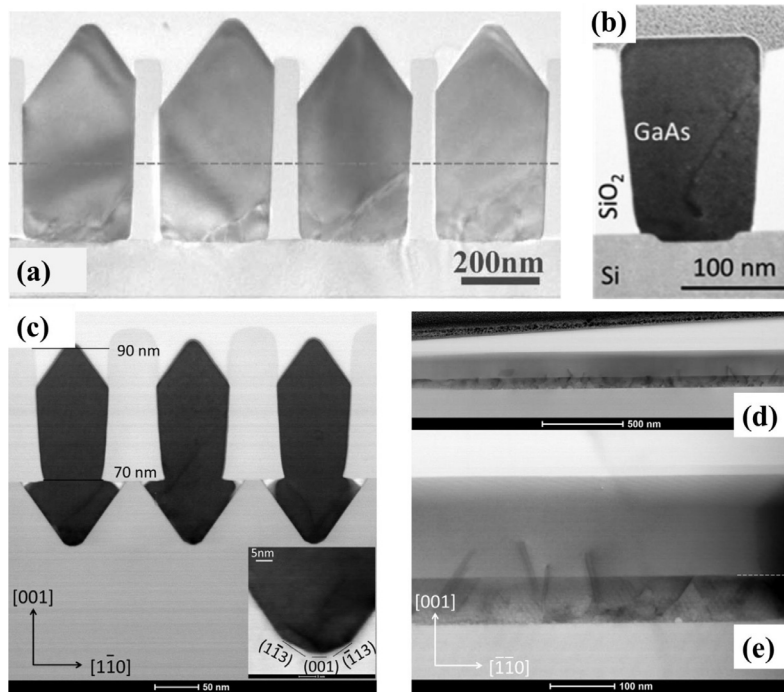


**Fig. 10.** (a) Tilted-view SEM image of GaAs selectively grown on a stripe patterned  $(001)$  Si substrate. (b) Cross-sectional annular dark field STEM image of GaAs-on-sub-micron-patterned-Si, showing the propagation of dislocations and stacking faults.

$[111]$ .

Within the ART approach, engineering the Si surface at the bottom of the trenches is critical. Realizing an oxide-free III-V/Si interface and minimizing the bottom trench roughness are effective in improving morphology uniformity and reducing twin defects. However, it is still difficult to control APD generation on a flat  $(001)$  Si surface. The



density of defects such as twin planes travelling along the trench direction is fairly high. By etching Si in alkaline solutions (such as potassium hydroxide, tetramethylammonium hydroxide or ammonium hydroxide), Si V-grooves are formed as a result of the lowest Si etch rates in {111} planes. Growing III-V materials on V-grooved (111) Si surfaces can greatly enhance the quality of epitaxial III-V materials in the ART process [112,113]. Fig. 11(c)–(e) display bright field STEM images of GaAs-on-V-grooved-Si in directions both perpendicular and parallel to the trenches. All threading dislocations (meandering lines) are found annihilated on the oxide walls and confined at the trench bottom. Very few {111} planar defects can be identified and none of them reach the surface, suggesting the upper part of the inspected GaAs portion is free of defects.

Integration of InP and associated alloys on Si by the ART method is of great interest for device applications ranging from high mobility transistors to emitters at telecom wavelengths. However, the 8% lattice mismatch between InP on Si poses a big challenge. With a high surface mobility of the Indium adatom, InP/Si nucleation in nanosized regions can have significant spatial non-uniformity [114]. Fig. 12 summarizes four growth schemes that have been investigated in the past few years. In Fig. 12(a), InP growth is performed on rounded Ge surfaces

[115,116]. The surface steps of the Si and Ge are carefully engineered to avoid APDs. A high-density dislocation network appears at the InP/Ge hetero-interfaces. According to results of FinFETs fabricated on such a material platform, out diffusion of Ge into the InP layer generates severe buffer leakage current, compromising transistor on-off ratios. Fig. 12(b) shows direct growth of InP on V-grooved Si using a low nucleation temperature and an extremely high V/III ratio of larger than 2000 [114]. TEM and x-ray diffraction (XRD) characterizations suggest greatly enhanced crystalline quality as compared to the InP-Ge-Si structure. By mimicking metamorphic InP/GaAs buffer on planar Si [55,66], Fig. 12(c) illustrates the use of a GaAs intermediate layer [117,118]. It eases the difficulty in subsequent InP epitaxy because of the halved lattice mismatch. This GaAs layer filling up the entire V-shaped Si pockets, however, decreases effective aspect ratio for defect trapping. It was found that a thick GaAs transitional buffer might not be necessary. In the design of Fig. 12(d), a low-temperature GaAs nucleation layer which is only a-few-nanometer thick is deposited prior to InP epitaxy [119,120]. Compared to the structure in Fig. 12(b), similar crystalline quality is achieved under much more relaxed growth conditions.

The use of {111} Si v-grooves in the ART growth process clearly demonstrates its unique advantages. First, the crystallographic alignment between the Si and III-V materials in the V-grooves avoids the introduction of APDs. Fig. 13(a) shows a III-V lattice in the V-shape of Si with {111} facets along the [110] direction [121]. Crystallography analysis indicates that the III-V semiconductors on the two {111} facets of the “V-shape” have the same polarity. In principle, the Si (111) surface can also have surface steps, as in the case of Si (001). However, a single step on the Si (111) surface has the height of one Si (111) double-layer (0.31 nm) [122,123]. As shown in Fig. 13(b), such steps will not lead to the formation of APBs. Secondly, III-V nucleation on Si (111) generates less defects as compared to nucleation on Si (001). For InP epitaxy on Si (111), under proper growth conditions, the large lattice mismatch can be mostly absorbed by a thin layer of one dimensional twins that are parallel to the growth surface [114,119,121]. This is in sharp contrast to the hetero-epitaxy on the Si (001) surface in which stress is mainly relaxed by misfits and 60° threading dislocations.

Growing III-V crystals in nano-sized cavities by the ART technique offers a viable path to integrate III-V high-mobility channel materials

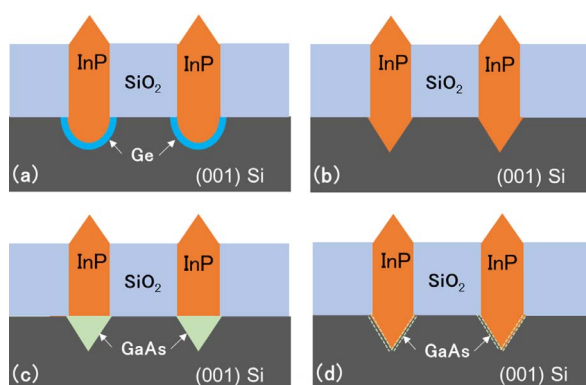


Fig. 12. Four epitaxial schemes of InP on ART patterned Si: (a) InP on rounded Ge surface; (b) direct InP epitaxy on V-grooved Si; (c) InP on a GaAs intermediate buffer filling up the V-grooves; (d) InP on a few-nanometer-thick GaAs stress relaxing layer.

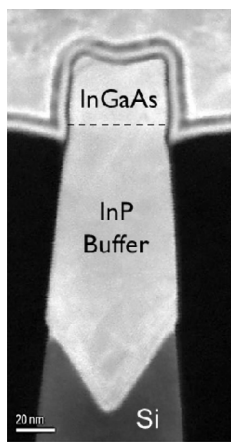
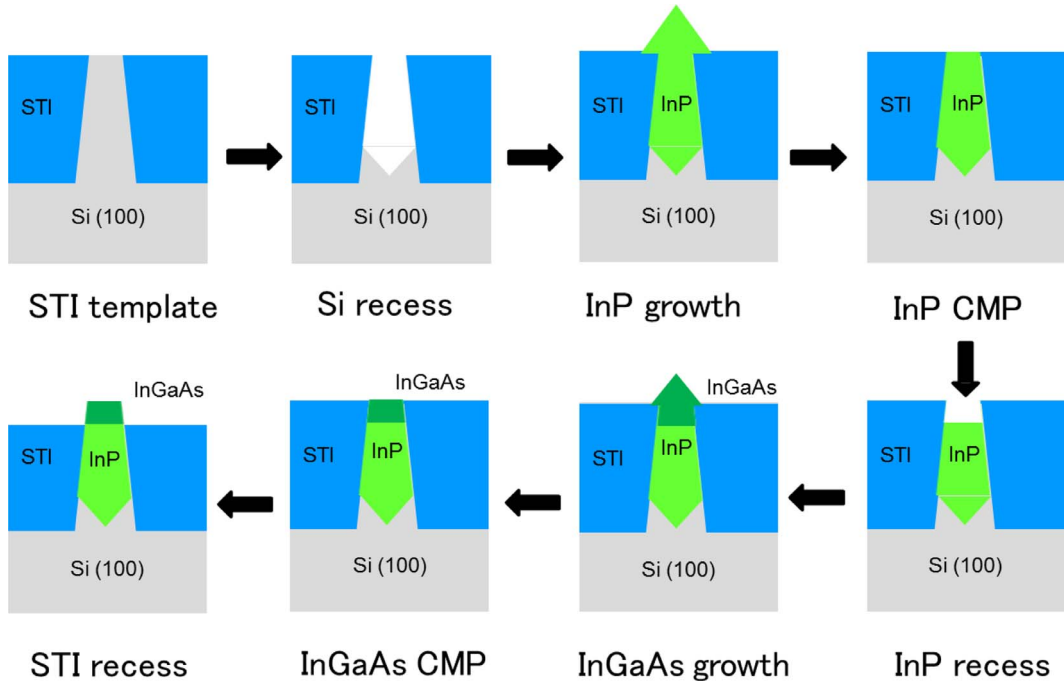
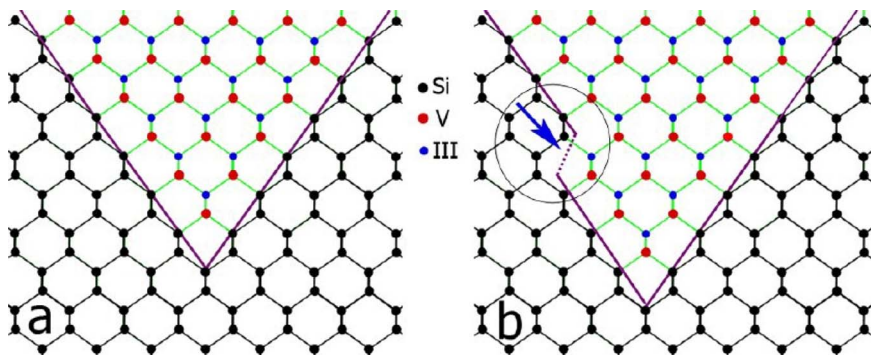
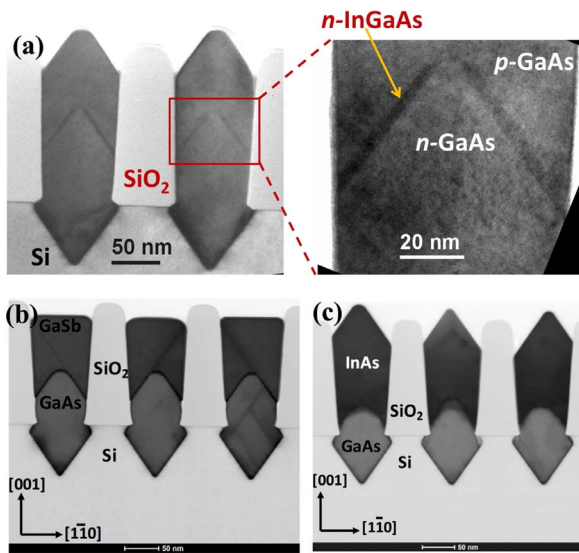


Fig. 15. DF-STEM of a 50 nm InGaAs fin formed by the replacement fin process. [124].

into advanced CMOS technology. A replacement fin process (See Fig. 14) was recently developed to fabricate InGaAs FinFETs on 300 mm Si substrates [124]. A sequence of epitaxial growth and CMP steps were used to form the InGaAs channel. After the shallow trench isolation (STI) template formation, the dummy Si was removed and MOCVD growth was performed to fill up the STI trench with InP buffer. The first

CMP step was then applied to get a flat InP surface. This was followed by recess etching which ultimately determines the height of the InGaAs fin. The InGaAs channel was then grown and the Indium content target is 53% to be lattice matched to the InP. The InGaAs was planarized by a second CMP step and the fin was revealed by recessing of the STI oxide. This process, where defects are trapped at the STI sidewall, led to the first realization of III-V FinFETs (see Fig. 15) with well-behaved on-off characteristics on large scale Si wafers in a fully VLSI compatible flow. It was later applied to fabricate various other transistor structures incorporating III-V high mobility channels. By removing the leaky InP buffer layer from underneath the InGaAs channel, InGaAs gate-all-around (GAA) and nanowire transistors [125] have been demonstrated on the same platform, showing greatly enhanced performance.

In addition to GaAs/Si and InP/Si integration, the application of the ART technique extends to ternary alloys, hetero-structures and 6.1 Å family heteroepitaxial layers. The cross-sectional TEM image in Fig. 16(a) shows the structure of a new type of GaAs-InGaAs-GaAs fin-array Esaki tunnel diode fabricated on (001) Si substrates using the ART integration process [126]. A room-temperature peak-to-valley current ratio (PVCR) of 5.4 is obtained and negative differential resistance characteristics remain up to 200 °C. Such fin-array tunnel diodes, serving as the building blocks, are used to form inverters [127] and fin-array tunneling triggers with tunable hysteresis [128], demonstrating potential logic applications. GaSb and InAs are materials of interest for



**Fig. 16.** (a) Cross-sectional TEM images of the GaAs-InGaAs-GaAs tunnel diode. The zoomed-in image presents the QW structure. [126] (b) Bright field STEM image of a cross-section of GaSb on GaAs-on-Si fins [129]. (c) Bright field STEM image of a cross-section of InAs on GaAs on Si fins [129].

high-mobility p-channel and n-channel transistors, respectively. The broken-gap band alignments formed by their hetero-structures could be exploited for novel tunnel FETs with steep subthreshold swings. Fig. 16(b) and (c) present TEM images of GaSb and InAs fins grown on top of GaAs fins on Si [129]. These results highlight the flexibility of the ART process in heterogeneous materials integration and its potential in co-integration of n-channel and p-channel FinFETs based on high-mobility 6.1 Å family compound semiconductors.

The aforementioned nano-scale selective epitaxy shows promise for next generation logic transistors. Substantial efforts are being made to leverage the same technique for integrated photonic devices requiring a large material volume for a sufficient modal gain. In one approach, III-V materials are grown out of tiny trenches to form bigger structures. Fig. 17(a) and (b) show SEM images of GaAs box-shaped ridges by this method [109]. The straight and uniform ridges with flat surfaces in all directions are promising for realizing waveguides with low light scattering losses. Compressively strained InGaAs/GaAs MQWs are deposited on top of the fully relaxed GaAs ridges, exhibiting pronounced QW photoluminescence at room-temperature. Fig. 17(c) illustrates a

similar epitaxial scheme, but to grow tilted InP nanowires out of nano-trenches on a patterned  $\text{SiO}_2$ -on-Si substrate [130]. The nanowires, with a hexagonal top, consist of a mixture of wurtzite and zincblende crystal phases, forming type II hetero-structures that promote lasing over a wide wavelength range. An alternative path to integrate III-V structures on Si with sufficient volume for laser cavities is to use a relatively large trench size. Fig. 17(d) presents highly ordered InP ridges selectively grown on sub-micron V-groove-patterned Si [119]. Quantum wires and ridge QW [120] structures emitting at telecom wavelengths have been demonstrated. Fig. 17(e) schematically depicts the fabrication of an InP distributed feedback laser array on Si using the selective-area growth technique in confined regions and top-down lithographic patterning [131]. Compared to other integration schemes, this result presents a highly scalable monolithic solution compatible with standard high-volume and low-cost CMOS manufacturing processes.

Recently, an alternative to the ART technique known as the confined epitaxial lateral overgrowth (CELO) technique [132] has been developed. This method begins with the formation of a 3D cavity in an oxide containing a crystalline seed. The 3D cavity is then selectively filled by the epitaxial material, during which the growth direction is forced to turn 90° (from vertical to lateral) with respect to the original seed. For traditional ART, planar defects traveling along the trench cannot be filtered geometrically, whereas defect trapping in CELO occurs in two directions and all defects are presumably confined in the seed region by geometry (see Fig. 18(a)). Compared to classical epitaxial lateral overgrowth, growth by CELO is constrained in a cavity that is pre-defined by a sacrificial layer. As a result, the epilayer thickness and morphology are well controlled. A smooth surface can be achieved without the need for CMP. Fig. 18(b)–(f) show typical SEM and TEM images of InGaAs CELO for scalable integration of CMOS-compatible InGaAs-on-insulator MOSFETs on large-area Si substrates.

Combining the ART technique with epitaxial lateral overgrowth (ELOG) is able to provide large regions of device materials. A new monolithic integration platform based on InP ELOG technology has been proposed to integrate III-V lasers on Si, as shown in Fig. 19. A layer of InP is first deposited on planar Si wafers and then polished by CMP. Micro-sized  $\text{SiO}_2$  stripe patterns are defined for the subsequent InP ELOG. The method exploits the  $\text{SiO}_2$  mask to filter the dislocations at the same time as the waveguide layer, enabling the integration of a monolithic evanescently coupled silicon laser (MECSL) [133]. High-quality QWs have been successfully grown on the ELOG InP layers, exhibiting comparable light emission intensities (> 85%) to those on a

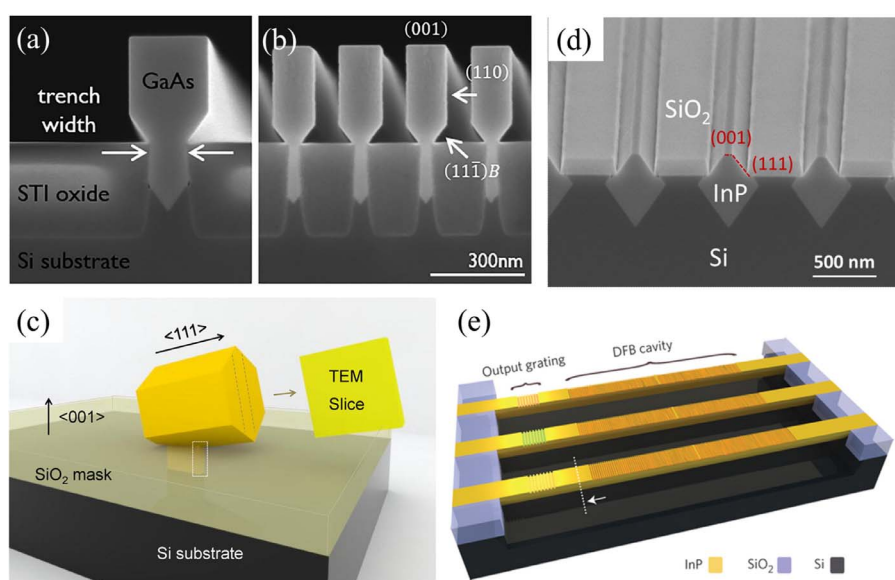


**Fig. 17.** (a) SEM pictures of box-shaped ridges (100 nm wide trench) integrated on STI-patterned Si wafers [109]. (b) SEM pictures of box-shaped ridges (20 nm wide trench) integrated on STI-patterned Si [109]. (c) A schematic configuration of the InP nanolaser epitaxially grown on (001) silicon. [130] (d) Tilted SEM image showing highly ordered InP nano ridges separated by  $\text{SiO}_2$  spacers [119]. (e) Schematic of the monolithically integrated InP DFB lasers on Si. The laser cavities and the output gratings are labelled. Differently colored output gratings illustrate the tunability of the lasing wavelength [131]. (For interpretation of the references to colour in this figure legend, the reader is referred to the web version of this article.)

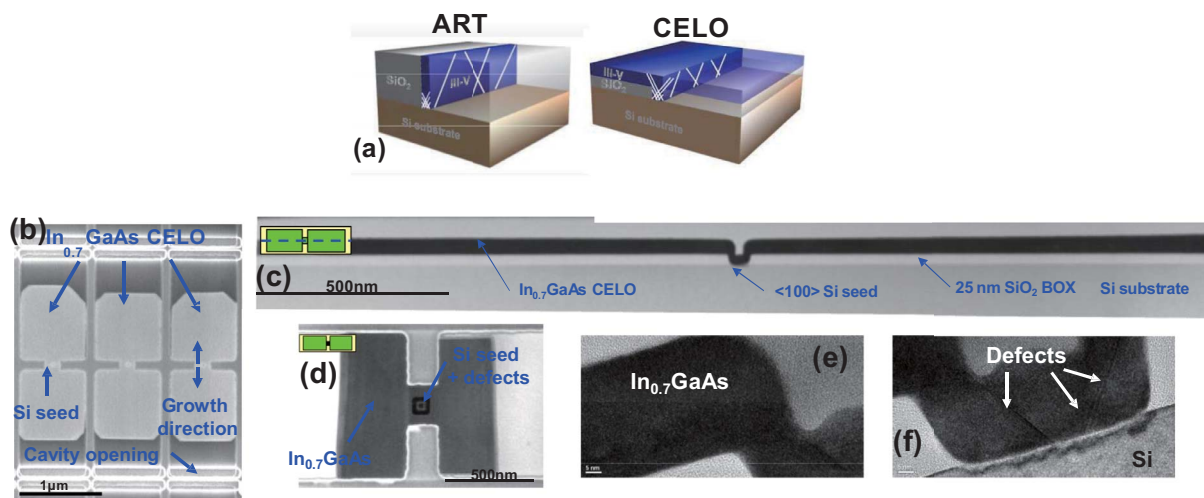


**Fig. 18.** (a) Comparison of the CELO approach with traditional ART. By forcing the growth direction to turn 90° with respect to the original seed, defect trapping occurs in two directions. For traditional ART, defects generated along the trench cannot be filtered geometrically. (b) Top-view SEM for In<sub>0.7</sub>Ga<sub>0.3</sub>As epitaxy into CELO structures. (c) TEM cross-sectional view of the corresponding InGaAs CELO structure highlighting the long and thin InGaAs region on a 25 nm buried oxide and the Si seed region. (d) Plan-view and (e,f) cross-sectional HRTEM images confirming that crystalline defects are geometrically confined in the seed region [132]. (For interpretation of the references to colour in this figure legend, the reader is referred to the web version of this article.)

planar InP reference [134].

Selective-area hetero-epitaxy in conjunction with the ART technique has been used to realize various heterogeneous structures on Si. Yet large-area planar thin films are more amenable in some device applications [135]. Towards this goal, III-V materials are epitaxially grown out of closely spaced trenches and continued laterally on top of the oxide stripes until materials from adjacent trenches merge together. The resultant III-V on Si templates can be treated as virtual substrates (or compliant substrates) for subsequent epi-structure growth and device fabrication. Initial investigations of continuous GaAs films on SiO<sub>2</sub>-patterned Si substrates [136] discovered coalescence defects appearing in the form of threading dislocations, twin defects and stacking faults above the SiO<sub>2</sub> (Fig. 20(a) and (b)). This was accompanied by a rough crystallographic surface. A two-temperature step growth optimization was therefore implemented to reduce the coalescence defects, yielding an XRD  $\omega$ -rocking curve full-width-at-half-maximum (FWHM) of 190 arcsec for 1.5-μm GaAs on Si. However, the APD issue is not addressed and surface undulations are still visible (see Fig. 20(c)). CMP is generally required to establish a flat surface for device integration [137,138]. Despite various process modifications, reducing the coalescence dislocations remains an unsolved challenge [135].

An improved method to grow coalesced GaAs thin films on

patterned Si was demonstrated recently to produce GaAs-on-V-grooved Si (GoVS) templates [139]. It starts with an on-axis Si (001) substrate covered by a layer of SiO<sub>2</sub>. The SiO<sub>2</sub> is patterned by dry etching into [110] oriented stripes with a line opening of 90 nm and an oxide spacing of 40 nm. Then a 70 °C heated KOH solution (45%) is used to etch Si into diamond-shaped trenches bounded by {111} facets. After a pre-baking step in a MOCVD chamber, GaAs nanowires are formed by selective area hetero-epitaxy.

The SEM image in Fig. 21(a) presents the resultant highly ordered array of GaAs nanowires free of APDs. According to analysis of x-ray diffraction  $\omega$ -rocking curves, these nanowires with a thickness of 150 nm yield an FWHM comparable to that of 1 μm-thick GaAs thin films on planar off-cut Si. Fig. 21(b) displays a cross-sectional TEM image taken along the [110] zone axis. Only a few {111} plane stacking faults are observed in the bulk of the GaAs. The zoomed-in TEM image at the GaAs/Si hetero-interface indicates that the 4% lattice mismatch is accommodated by a few-nanometer-thick stacking disordered layer in parallel with the (111) growth surface. With this ultrathin GaAs stress relaxing layer, the GaAs bulk layer has a very high crystalline quality.

Looking more closely at the glide of the few-layer stacking faults/twins at the GaAs-Si hetero-interface reveals that the disordered layers are stopped by a “tiara” -like structure beneath the SiO<sub>2</sub> walls (see

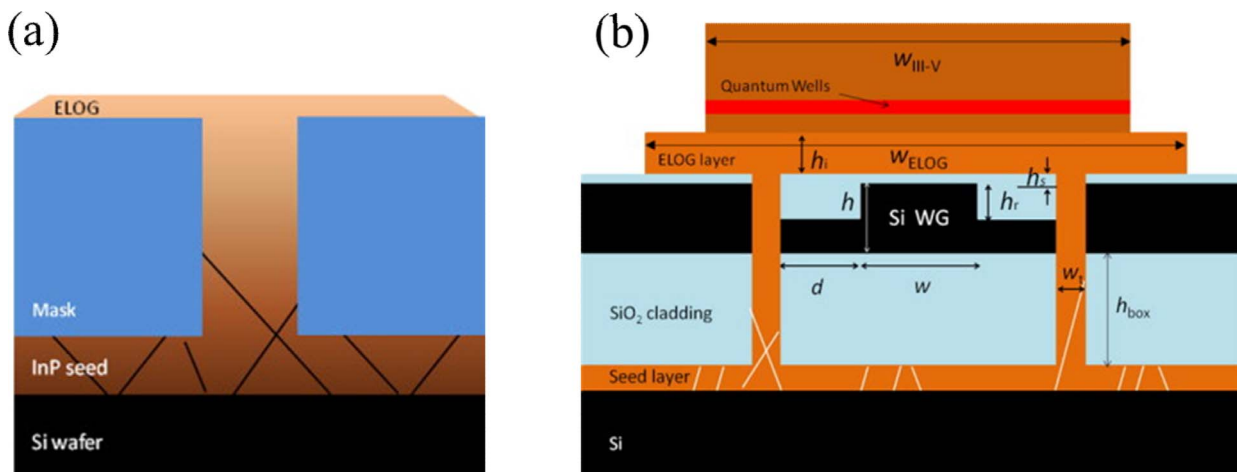


**Fig. 19.** Schematics of (a) epitaxial lateral overgrowth and (b) a monolithically evanescently coupled silicon laser (MECSL) structure based on the proposed integration platform [133].

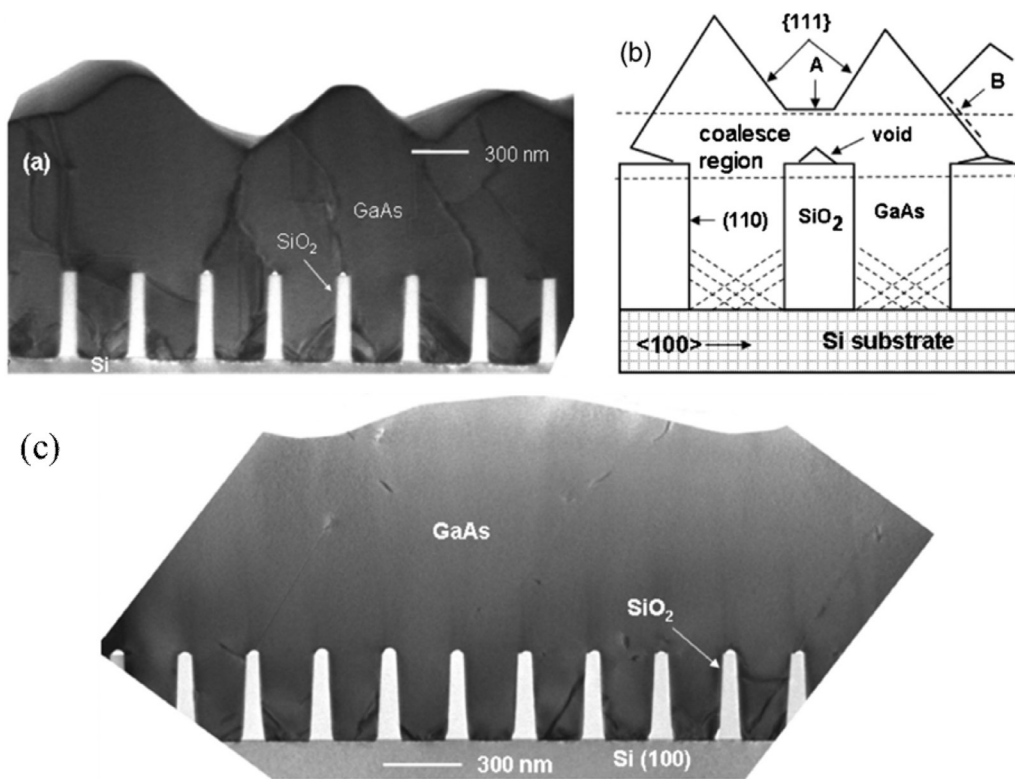


**Fig. 21(c)).** This “tiara” -like structure, made of Si, was formed together with the diamond-shaped Si pockets in the Si recessing process (the combination of dry etching and potassium hydroxide wet etching). This represents a slight modification from conventional simple Si V-grooves bounded by two {111} facets, but results in a unique defect trapping effect. Recall that in the conventional method [136] that combines ART growth within trenches and ELOG over SiO<sub>2</sub>, the SiO<sub>2</sub> stripes lead to a high density of coalescence defects and a high surface roughness. Here, with most of the hetero-interface defects stopped by the “tiara” structure, it is possible to remove the SiO<sub>2</sub> without jeopardizing the defect necking effect in the coalescence process. As shown in Fig. 22(a) and

(b), the GaAs nanowires without SiO<sub>2</sub> in between merged into a 300 nm planar GaAs film with a smooth surface. Fig. 22(c) schematically illustrates the defect trapping mechanism in the GaAs-on-V-grooved Si templates. The cross-sectional TEM image in Fig. 22(d) taken near the GaAs/Si interface confirms that most of the defects are confined within the diamond-shaped trenches. This growth method eliminates the necessity to use misoriented Si substrates or graded SiGe/Ge buffers, and erases the difficulties in achieving coalescence over dielectric patterns. A flat planar film can be obtained in a simpler way without an additional CMP planarization process. It was found later that, with the insertion of AlGaAs/GaAs or InGaAs/GaAs superlattices in the GaAs, the

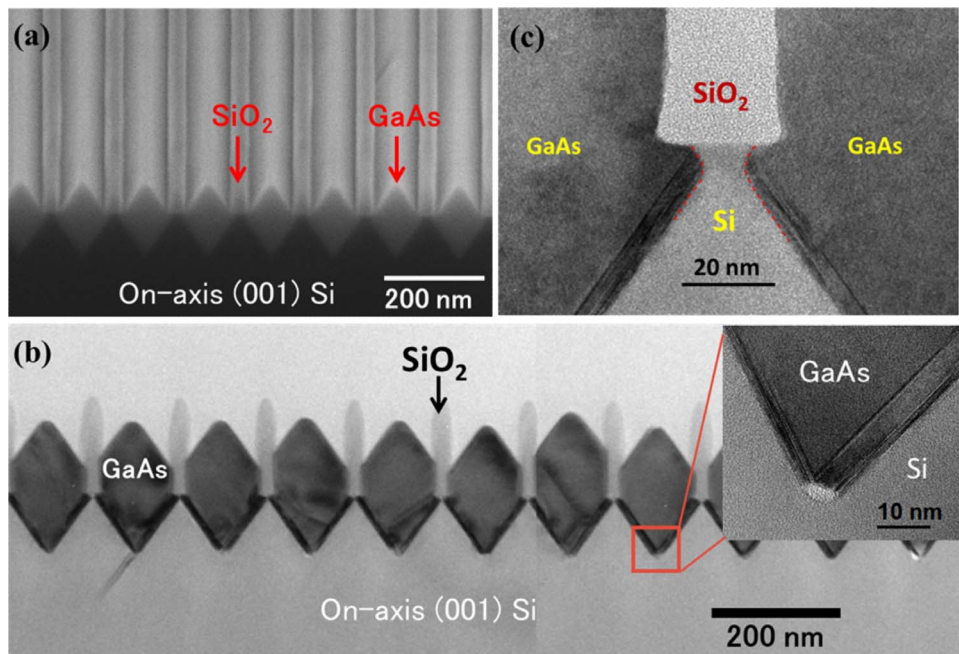


**Fig. 21.** (a) SEM image of array of in-plane GaAs nanowires on V-grooved Si separated by SiO<sub>2</sub> spacers. (b) Cross-sectional TEM image of the array of GaAs nanowires taken along the [110] zone axis. The zoomed-in image highlights the GaAs/Si hetero-interface. (c) The few-layer stacking faults/twins at the GaAs-silicon hetero-interface under TEM reveal that the disordered layers are stopped by a “tiara”-like structure beneath the SiO<sub>2</sub> walls [139]. (For interpretation of the references to colour in this figure legend, the reader is referred to the web version of this article.)

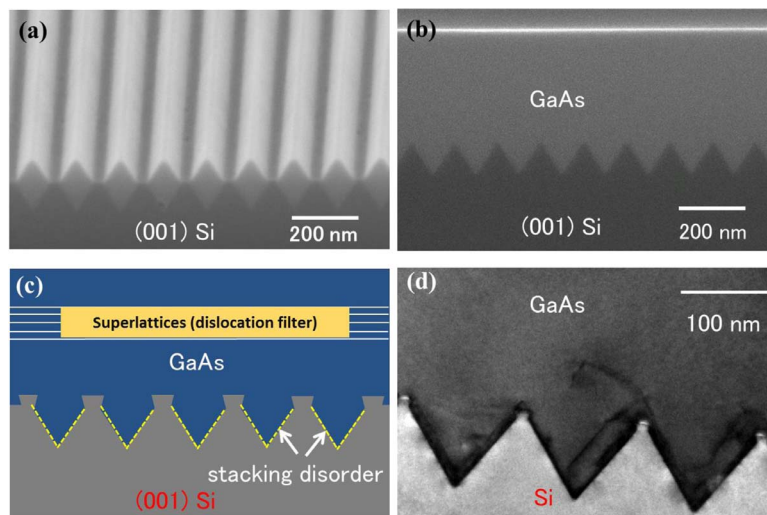


**Fig. 22.** (a) Tilted SEM image showing an array of GaAs with  $\text{SiO}_2$  spacers removed prior to III-V overgrowth. (b) Cross-sectional SEM image of 300-nm coalesced GaAs with a flat surface [139]. (c) The defect trapping mechanism for GaAs-on-V-grooved Si templates. (d) Cross-sectional TEM image taken near the GaAs/Si interface showing most of the crystal defects are localized and trapped within the diamond-shaped pockets.

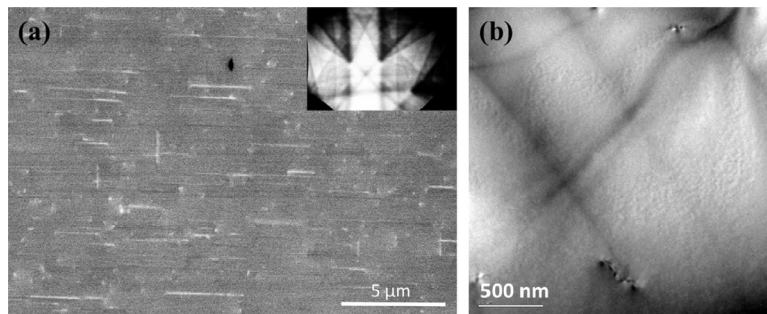


**Fig. 23.** (a) Plan-view electron channeling contrast image (ECCI) of a GaAs-on-v-grooved-Si template. The bright dashes are attributed to stacking faults, while the pinpoints represent threading dislocations intersecting the sample surface. Counting reveals a threading dislocation density of  $7 \times 10^7 \text{ cm}^{-2}$  and a stacking fault density of  $2 \times 10^7 \text{ cm}^{-2}$ . (Inset) The electron channeling pattern corresponding to the (220) and (020) imaging condition used. [105] (b) A plan-view TEM image of a GaAs-on-v-groove-Si template.

root-mean-square roughness of the GoVS templates across an area of  $10 \times 10 \mu\text{m}^2$  can be lowered to less than 1 nm [105].

The defect densities of the GoVS templates have been assessed through electron channeling contrast imaging (ECCI) [105], plan-view TEM and x-ray rocking curves. ECCI uses a scanning electron microscope in backscatter mode at a given diffraction condition to image deviations from the Bragg condition caused by strain fields, such as those around dislocations and local phase shifts of the electron wave caused by the non-integer lattice translations across stacking faults. It allows for rapid acquisition of large-area scans without any material preparation. For a 2  $\mu\text{m}$  GoVS, a threading dislocation density of  $7 \times 10^7 \text{ cm}^{-2}$  and a stacking fault density of  $2 \times 10^7 \text{ cm}^{-2}$  are obtained from the ECCI image in Fig. 23(a). A plan-view TEM image of a typical GoVS template in Fig. 23(b) suggests a dislocation density in the order of  $10^7 \text{ cm}^{-2}$ , which is consistent with ECCI characterization. The GoVS templates provide opportunities for integration of electronic, photonic, or photovoltaic devices on Si wafers. InAs/GaAs QD structures grown on the GoVS template show superior optical properties as compared to those grown on planar offcut Si [140], while optically pumped micro-disk lasers fabricated on the GoVS templates exhibit promisingly low threshold lasing characteristics [141–143]. Electrically injected, Fabry-Perot, QD ridge lasers on the GoVS templates were also reported, showing CW operation up to 80 °C, with threshold currents as low as 37 mA [105]. Applying a similar growth technique to develop InP and other III-V on Si virtual substrates is of great interest for future studies.

## 5. Summary

Monolithic III-V/Si integration can leverage the best physical properties of III-V devices with the advanced manufacturing process associated with silicon. Emerging technologies and applications provide new driving forces to transform this concept into an industrial solution. Notable progress has been made recently in developing novel epitaxial

schemes as well as in overcoming the persistent challenges in material mismatch. Proof-of-principle demonstrations from exploratory transistors to on-chip quantum-dot lasers suggest good performance gain and integration potential. Efforts should continue to be devoted to resolving the compatibility of integration techniques with large-volume CMOS manufacturing, addressing device reliability issues and designing integrated systems.

## Acknowledgements

This work was supported in part by an Initiation Grant (IGN15EG01) from HKUST and the Innovation Technology Fund of Hong Kong (No. ITS/273/16FP). We want to acknowledge Bei Shi, Yu Han and Yating Wan for discussions of results.

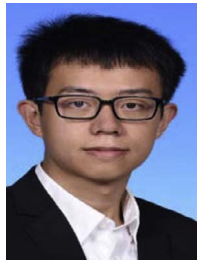
## Reference

- [1] E.A. Fitzgerald, M.T. Balsara, Y. Bai, C. Cheng, W.K. Liu, D. Lubyshev, J.M. Fastenau, Y. Wu, M. Urtega, W. Ha, J. Bergman, Monolithic III-V/Si Integration, *ECS Trans.* 16 (10) (2008) 1015–1020.
- [2] J.A. del Alamo, Nanometre-scale electronics with III-V compound semiconductors, *Nature* 479 (2011) 317–323.
- [3] D. Liang, J.E. Bowers, Recent progress in lasers on silicon, *Nat. Photonics* 4 (2010) 511–517.
- [4] I. Németh, B. Kunert, W. Stolz, K. Volz, Heteroepitaxy of GaP on Si: correlation of morphology, anti-phase-domain structure and MOVPE growth conditions, *J. Cryst. Growth* 310 (7) (2008) 1595–1601.
- [5] K. Volz, A. Beyer, W. Witte, J. Ohlmann, I. Nemeth, B. Kunert, W. Stolz, Gap-nucleation on exact Si (0 0 1) substrates for III/V device integration, *J. Cryst. Growth* 315 (1) (2011) 37–47.
- [6] S. Liebich, M. Zimprich, A. Beyer, C. Lange, D.J. Franzbach, S. Chatterjee, N. Hossain, S.J. Sweeney, K. Volz, B. Kunert, W. Stolz, Laser operation of Ga (NAsP) lattice-matched to (001) silicon substrate, *Appl. Phys. Lett.* 99 (2011) 071109.
- [7] B. Kunert, S. Zinnkann, K. Volz, W. Stolz, Monolithic integration of Ga(NAsP)/(BGa)P multi-quantum well structures on (0 0 1) silicon substrate by MOVPE, *J. Cryst. Growth* 310 (2008) 4776–4779.

- [8] P. Ludewig, S. Reinhard, K. Jandieri, T. Wegele, A. Beyer, L. Tapfer, K. Volz, W. Stoltz, MOVPE growth studies of Ga(NAsP)/(BGa)(AsP) multi quantum well heterostructures (MQWH) for the monolithic integration of laser structures on (001) Si-substrates, *J. Crys. Growth* 438 (2016) 63–69.
- [9] C.J.K. Richardson, M.L. Lee, Metamorphic epitaxial materials, *MRS Bull.* 41 (2016) 193.
- [10] C.W. Liu, M. Ostling, J.B. Hannon, New materials for post-Si computing, *MRS Bull.* 39 (8) (2014) 658–662.
- [11] M. Sugo, H. Mori, Y. Itoh, Y. Sakai, M. Tachikawa, 1.5  $\mu\text{m}$ -long-wavelength multiple quantum well laser on a Si substrate, *Jpn. J. Appl. Phys.* 30 (12S) (1991) 3876.
- [12] T. Yamada, M. Tachikawa, T. Sasaki, H. Mori, Y. Kadota, 7000 h continuous wave operation of multiple quantum well laser on Si at 50 °C, *Appl. Phys. Lett.* 70 (1997) 1614.
- [13] V.K. Yang, M. Groenert, C.W. Leitz, A.J. Pitera, M.T. Currie, E.A. Fitzgerald, Crack formation in GaAs heteroepitaxial films on Si and SiGe virtual substrates, *J. Appl. Phys.* 93 (2003) 3859.
- [14] S.H. Huang, G. Balakrishnan, A. Khoshakhlagh, A. Jallipalli, L.R. Dawson, D.L. Huffaker, Strain relief by periodic misfit arrays for low defect density GaSb on GaAs, *Appl. Phys. Lett.* 88 (2006) 131911.
- [15] J. Tatebayashi, A. Jallipalli, M.N. Kutty, S.H. Huang, G. Balakrishnan, L.R. Dawson, D.L. Huffaker, Structural analysis of highly relaxed GaSb grown on GaAs substrates with periodic interfacial array of 90° misfit dislocations, *Appl. Phys. Lett.* 91 (2007) 141102.
- [16] S. Huang, G. Balakrishnan, D.L. Huffaker, Interfacial misfit array formation for GaSb growth on GaAs, *J. Appl. Phys.* 105 (2009) 103104.
- [17] W. Zhou, W. Tang, K.M. Lau, A strain relief mode at interface of GaSb/GaAs grown by metalorganic chemical vapor deposition, *Appl. Phys. Lett.* 99 (2011) 221917.
- [18] K. Akahane, N. Yamamoto, S.I. Gozu, N. Ohtani, Heteroepitaxial growth of GaSb on Si(0 0 1) substrates, *J. Crys. Growth* 264 (2004) 21.
- [19] E. Tournié, L. Cerutti, J.B. Rodriguez, H. Liu, J. Wu, S. Chen, Metamorphic III-V semiconductor lasers grown on silicon, *MRS Bull.* 41 (03) (2016) 218.
- [20] G. Balakrishnan, S.H. Huang, A. Khoshakhlagh, A. Jallipalli, P. Rotella, A. Amtout, S. Krishna, C.P. Haines, L.R. Dawson, D.L. Huffaker, Room-temperature optically-pumped GaSb quantum well based VCSEL monolithically grown on Si (100) substrate, *Electr. Lett.* 42 (2006) 350.
- [21] J. Tatebayashi, A. Jallipalli, M.N. Kutty, S. Huang, K. Nunna, G. Balakrishnan, L.R. Dawson, D.L. Huffaker, Monolithically integrated III-Sb-based laser diodes grown on miscut Si substrates, *IEEE J. Sel. Top. Quant. Electron.* 15 (2009) 716.
- [22] G. Balakrishnan, A. Jallipalli, P. Rotella, S. Huang, A. Khoshakhlagh, A. Amtout, S. Krishna, L.R. Dawson, D.L. Huffaker, Room-temperature optically pumped (Al)GaSb vertical-cavity surface-emitting laser monolithically grown on an Si(1 0 0) substrate, *IEEE J. Sel. Top. Quant. Electron.* 12 (2006) 1636.
- [23] L. Cerutti, J.B. Rodriguez, E. Tournie, GaSb-based laser, monolithically grown on silicon substrate, emitting at 1.55  $\mu\text{m}$  at room temperature, *IEEE Photonics Technol. Lett.* 22 (8) (2010) 553.
- [24] J.R. Reboul, L. Cerutti, J.B. Rodriguez, P. Grech, E. Tournie, Continuous-wave operation above room temperature of GaSb-based laser diodes grown on Si, *Appl. Phys. Lett.* 99 (2011) 121113.
- [25] A. Castellano, L. Cerutti, J.B. Rodriguez, G. Narcy, A. Garreau, F. Lelarge, E. Tournie, Room-temperature continuous-wave operation in the telecom wavelength range of GaSb-based lasers monolithically grown on Si, *APL Photonics* 2 (2017) 061301.
- [26] D. Jena, Polarization Induced Electron Populations in III-V Nitride Semiconductors: Transport, Growth, and Device Applications, Dept. Electrical and Computer Engineering, UCSB, CA, USA, 2003.
- [27] J. Faucher, T. Masuda, M.L. Lee, Initiation strategies for simultaneous control of antiphase domains and stacking faults in GaAs solar cells on Ge, *J. Vac. Sci. Technol. B Nanotechnol. Microelectr.* 34 (4) (2016) 041203.
- [28] G. Brammertz, Y. Mols, S. Degroote, V. Mototsnyi, M. Leyts, G. Borghs, M. Caymax, Low-temperature photoluminescence study of thin epitaxial GaAs films on Ge substrates, *J. Appl. Phys.* 99 (9) (2006) 093514.
- [29] R. Alcotte, M. Martin, J. Moeyaert, R. Cipro, S. David, F. Bassani, F. Ducroquet, Y. Bogumilowicz, E. Sanchez, Z. Ye, X. Bao, J. Pin, T. Baran, Epitaxial growth of antiphase boundary free GaAs layer on 300 nm Si (001) substrate by metalorganic chemical vapour deposition with high mobility, *APL Mater.* 4 (4) (2016) 046101.
- [30] M. Akiyama, Y. Kawarada, K. Kaminiishi, Growth of single domain GaAs layer on (100)-oriented Si substrate by MOCVD, *Jpn. J. Appl. Phys.* 23 (1984) L843.
- [31] H. Kroemer, MBE growth of GaAs on Si: problems and progress, *Mat. Res. Soc. Symp. Proc.* 67 (1986) 3.
- [32] W.A. Harrison, E.A. Kraut, J.R. Waldrop, R.W. Grant, Polar heterojunction interfaces, *Phys. Rev. B* 18 (8) (1978) 4402.
- [33] S.J. Pearton, D.L. Malm, L.A. Heimbrock, J. Kovalchick, C.R. Abernathy, R. Caruso, S.M. Vernon, V.E. Haven, Heterointerface stability in GaAs on Si grown by metalorganic chemical vapor deposition, *Appl. Phys. Lett.* 51 (1987) 682.
- [34] S.J. Pearton, C.R. Abernathy, F. Ren, Topics in growth and device processing of III-V semiconductors, *World Sci.* 1 (1996) 141–144.
- [35] S.F. Fang, K. Adomi, S. Iyer, H. Morkoc, H. Zabel, Gallium arsenide and other compound semiconductors on silicon, *J. Appl. Phys.* 68 (1990) R31.
- [36] M. Akiyama, Y. Kawarada, K. Kaminiishi, Growth of GaAs on Si by MOVCD, *J. Cryst. Growth* 68 (1984) 21–26.
- [37] H. Morkoc, C.K. Peng, T. Henderson, W. Kopp, R. Fischer, L.P. Erickson, M.D. Longerborn, R.C. Youngman, High-quality GaAs MESFET's grown on silicon substrates by molecular-beam epitaxy, *IEEE Electron Dev. Lett.* 6 (1985) 381.
- [38] M. Kawabe, T. Ueda, Molecular beam epitaxy of controlled single domain GaAs on Si (100), *Jpn. J. Appl. Phys.* 25 (4) (1986) L285.
- [39] D.J. Chadi, Stabilities of single-layer and bilayer steps on Si(001) surfaces, *Phys. Rev. Lett.* 59 (1987) 1691.
- [40] J.W. Lee, H. Shichijo, H.L. Tsai, R.J. Matyi, Defect reduction by thermal annealing of GaAs layers grown by molecular beam epitaxy on Si substrates, *Appl. Phys. Lett.* 50 (1987) 31.
- [41] M. Yamaguchi, Dislocation density reduction in heteroepitaxial III-V compound films on Si substrates for optical devices, *J. Mater. Res.* 6 (1991) 376.
- [42] M. Yamaguchi, A. Yamamoto, M. Tachikawa, Y. Itoh, M. Sugo, Defect reduction effects in GaAs on Si substrates by thermal annealing, *Appl. Phys. Lett.* 53 (1988) 2293.
- [43] C-W Hsu, Y-F Chen, Y-K Su, Nanoepitaxy of GaAs on a Si(001) substrate using a round-hole nanopatterned SiO<sub>2</sub> mask, *Nanotechnology* 23 (2012) 495306.
- [44] M. Yamaguchi, T. Nishioka, M. Sugo, Analysis of strained layer superlattice effects on dislocation density reduction in GaAs on Si substrates, *Appl. Phys. Lett.* 54 (1989) 24.
- [45] Y. Takano, M. Hisaka, N. Fujii, K. Suzuki, K. Kuwahara, S. Fuke, Reduction of threading dislocations by InGaAs interlayer in GaAs Layers grown on Si substrates, *Appl. Phys. Lett.* 73 (1998) 2917–2919.
- [46] E.A. Fitzgerald, Y.H. Xie, M.L. Green, D. Brasen, A.R. Kortan, J. Michel, Y.J. Mii, B.E. Weirless, Totally relaxed Ge<sub>x</sub>Si<sub>1-x</sub> layers with low threading dislocation densities grown on Si substrates, *Appl. Phys. Lett.* 59 (1991) 811–813.
- [47] C.L. Andre, J.A. Carlin, J.J. Boeckl, D.M. Wilt, M.A. Smith, A.J. Pitera, M.L. Lee, E.A. Fitzgerald, S.A. Ringel, Investigations of high-performance GaAs solar cells grown on Ge-Si<sub>x</sub>-Ge<sub>x</sub>Si substrates, *IEEE Trans. Electron Dev.* 52 (2005) 1055.
- [48] M. González, C.L. Andre, R.J. Walters, S.R. Messenger, J.H. Warner, J.R. Lorentzen, A.J. Pitera, E.A. Fitzgerald, S.A. Ringel, Deep level defects in proton radiated GaAs grown on metamorphic SiGe/Si substrates, *J. Appl. Phys.* 100 (2006) 034503.
- [49] Y. Bolkhovityanov, O. Pchelyakov, GaAs epitaxy on Si substrates: modern status of research and engineering, *Phys. Uspekhi* 51 (5) (2008) 437–456.
- [50] T. Roesener, H. Dösscher, A. Beyer, S. Brückner, V. Klinger, A. Wekkeli, P. Kleinschmidt, C. Jurecka, J. Ohlmann, K. Volz, W. Stoltz, MOVPE growth of III-V solar cells on silicon in 300 mm closed coupled showerhead reactor, 25th European Photovoltaic Solar Energy Conf. and Exhibition, 2010, pp. 964–968.
- [51] <http://www.nasp.de/>.
- [52] K.N. Yaung, J.R. Lang, M.L. Lee, Towards high efficiency GaAsP solar cells on (001) GaP/Si, *Proc. the IEEE 40th Photovoltaic Specialist Conference*, 2014, pp. 0831–0835.
- [53] K.N. Yaung, M. Vaisman, J. Lang, M.L. Lee, GaAsP solar cells on GaP/Si with low threading dislocation density, *Appl. Phys. Lett.* 109 (2016) 032107.
- [54] M.L. Huang, S.W. Chang, M.K. Chen, C.H. Fan, H.T. Lin, C.H. Lin, R.L. Chu, K.Y. Lee, M.A. Khaerbad, Z.C. Chen, C.H. Lin, C.H. Chen, L.T. Lin, H.J. Lin, H.C. Chang, C.L. Yang, Y.K. Leung, Y.-C. Yeo, S.M. Jang, H.Y. Hwang, C.H. Diaz, In<sub>0.53</sub>Ga<sub>0.47</sub>As MOSFETs with high channel mobility and gate stack quality fabricated on 300 nm Si substrate, *IEEE Symposium on VLSI Technology*, 2015, pp. T204–T205.
- [55] T. Orzali, A. Vert, T.-W. Kim, P.Y. Hung, J.L. Herman, S. Vivekanand, G. Huang, M. Kelman, Z. Karim, R.J.W. Hill, S.S.P. Rao, Growth and characterization of an In<sub>0.53</sub>Ga<sub>0.47</sub>As-based metal-oxide-semiconductor capacitor (MOSCAP) structure on 300 nm on-axis Si (001) wafers by MOCVD, *J. Crys. Growth* 427 (2015) 72–79.
- [56] J.E. Ayers, The measurement of threading dislocation densities in semiconductor crystals by X-ray diffraction, *J. Cryst. Growth* 135 (1994) 71–77.
- [57] S. Takagi, M. Noguchi, M. Kim, S.-H. Kim, C.-Y. Chang, M. Yokoyama, K. Nishi, R. Zhang, M. Ke, M. Takenaka, III-V/Ge MOS device technologies for low power integrated systems, *Solid State Electr.* 125 (2016) 82–102.
- [58] V. Deshpande, V. Djara, E. O'Connor, P. Hashemi, T. Morf, K. Balakrishnan, D. Caimi, M. Sousa, J. Pompeyrine, L. Czornomaz, Three-dimensional monolithic integration of III-V and Si(Ge) FETs for hybrid CMOS and beyond, *Jpn. J. Appl. Phys.* 56 (2017) 04CA05.
- [59] S. Kim, Y. Ikuu, M. Yokoyama, R. Nakane, J. Li, Y.-C. Kao, M. Takenaka, S. Takagi, Direct wafer bonding technology for large-scale InGaAs-on-insulator transistors, *Appl. Phys. Lett.* 105 (2014) 043504.
- [60] N. Daix, E. Uccelli, L. Czornomaz, D. Caimi, C. Rossel, M. Sousa, H. Siegwart, C. Marchiori, J.M. Hartmann, K.T. Shiu, C.W. Cheng, Towards large size substrates for III-V co-integration made by direct wafer bonding on Si, *APL Mater.* 2 (2014) 086104.
- [61] V. Djara, V. Deshpande, E. Uccelli, N. Daix, D. Caimi, C. Rossel, M. Sousa, H. Siegwart, C. Marchiori, J.M. Hartmann, K.T. Shiu, An InGaAs on Si platform for CMOS with 200 nm InGaAs-OI substrate, gate-first, replacement gate planar and FinFETs down to 120 nm contact pitch, *Symp. VLSI Tech Dig.* (2015) T176–T177.
- [62] J. Widiez, S. Sollier, T. Baron, M. Martin, G. Gaudin, F. Mazen, F. Madeira, S. Favier, A. Salau, R. Alcotte, E. Beche, H. Grampeix, C. Veytizou, J.-S. Moulet, 300 nm InGaAs-on-insulator substrates fabricated using direct wafer bonding and the Smart Cut™ technology, *Jpn. J. Appl. Phys.* 55 (4S) (2016) 04EB10.
- [63] S. Brückner, H. Dösscher, P. Kleinschmidt, O. Supplie, A. Dobrich, T. Hannappel, Anomalous double-layer step formation on Si(100) in hydrogen process ambient, *Phys. Rev. B* 86 (2012) 195310.
- [64] Q. Li, C.W. Tang, K.M. Lau, Growth of ultra-high mobility In<sub>0.52</sub>Al<sub>0.48</sub>As/In<sub>x</sub>Ga<sub>1-x</sub>As (x ≥ 53%) quantum wells on Si substrates using InP/GaAs buffers by metal-organic chemical vapor deposition, *Appl. Phys. Expr.* 7 (4) (2014) 045502.
- [65] Y. Bogumilowicz, J.M. Hartmann, R. Cipro, R. Alcotte, M. Martin, F. Bassani, J. Moeyaert, T. Baron, J.B. Pin, X. Bao, Z. Ye, E. Sanchez, Anti-phase boundaries-free GaAs epilayers on “quasi-nominal” Ge-buffered silicon substrates, *Appl. Phys. Lett.* 107 (2015) 212105.
- [66] Q. Li, X. Zhou, C.W. Tang, K.M. Lau, Material and device characteristics of metamorphic In<sub>0.53</sub>Ga<sub>0.47</sub>As MOSHEMTs grown on GaAs and Si substrates by

- MOCVD, IEEE Trans. Electron Dev. 60 (12) (2013) 4112–4118.
- [67] Q. Li, H. Jiang, K.M. Lau, Coalescence of planar GaAs nanowires into strain-free three-dimensional crystals on exact (001) silicon, J. Crys. Growth 454 (2016) 19–24.
- [68] K.J. Kuhn, Considerations for ultimate CMOS scaling, IEEE Trans. Electron Dev. 59 (7) (2012) 1813–1828.
- [69] M.K. Hudait, G. Dewey, S. Datta, J.M. Fastenau, J. Kavalieros, W.K. Liu, D. Lubyshev, R. Pillarisetty, W. Rachmady, M. Radosavljevic, T. Rakshit, Heterogeneous integration of enhancement mode  $In_{0.7}Ga_{0.3}$ As quantum well transistor on silicon substrate using thin (less 2  $\mu$ m) composite buffer architecture for high-speed and low-voltage (0.5 logic applications), IEEE Int. Electron Devices Meet. (2007) 625–628.
- [70] N. Mukherjee, J. Boardman, B. Chu-Kung, G. Dewey, A. Eisenbach, J. Fastenau, J. Kavalieros, W.K. Liu, D. Lubyshev, M. Metz, K. Millard, MOVPE III-V material growth on silicon substrates and its comparison to MBE for future high performance and low power logic applications, IEEE Int. Electron Devices Meet. (2011) 35–1.
- [71] K.M. Lau, C.W. Tang, H. Li, Z. Zhong, AlInAs/GaInAs mHEMTs on silicon substrates grown by MOCVD, IEEE Int. Electron Devices Meet. (2008) 1–4.
- [72] Q. Li, X. Zhou, C.W. Tang, K.M. Lau, High-performance inverted  $In_{0.53}Ga_{0.47}$ As MOSHEMTs on a GaAs Substrate with regrown source/drain by MOCVD, IEEE Electron Device Lett. 33 (9) (2012) 1246–1248.
- [73] X. Zhou, Q. Li, C.W. Tang, K.M. Lau, Inverted-type InGaAs metal-oxide-semiconductor high-electron-mobility transistor on Si substrate with maximum drain current exceeding 2 A/mm, Appl. Phys. Express 5 (10) (2012) 104201.
- [74] X. Zhou, Q. Li, C.W. Tang, K.M. Lau, 30 nm inverted  $In_{0.53}Ga_{0.47}$ As MOSHEMTs on Si substrate grown by MOCVD with regrown source/drain, IEEE Electron Device Lett. 33 (10) (2012) 1384–1386.
- [75] X. Zhou, Q. Li, C.W. Tang, K.M. Lau, enhancement-mode  $In_{0.53}Ga_{0.47}$ As MOSFETs on Si substrates grown by MOCVD exhibiting high transconductance and low on-resistance, Int. Electron Devices Meet. 32 (2012) 5.
- [76] C.Y. Huang, X. Bao, Z. Ye, S. Lee, H. Chiang, H. Li, V. Chobpattana, B. Thibeault, W. Mitchell, S. Stemmer, A. Gossard, Ultrathin InAs-channel MOSFETs on Si substrates, International Symposium on VLSI Technology, Systems and Application (VLSI-TSA), 2015.
- [77] L. Virot, P. Crozat, J.M. Fédeli, J.M. Hartmann, D. Marras-Morini, E. Cassan, F. Boeuf, L. Vivien, Germanium avalanche receiver for low power interconnects, Nat. Commun. 5 (2014) 4957.
- [78] G.T. Reed, G. Mashanovich, F. Gardes, D. Thomson, Silicon optical modulators, Nat. Photon. 4 (2010) 518–526.
- [79] X. Luo, Y. Cao, J. Song, X. Hu, Y. Cheng, C. Li, C. Liu, T.-Y. Liow, M. Yu, H. Wang, Q.J. Wang, P. Lo, High-throughput multiple dies-to-wafer bonding technology and III/V-on-Si hybrid lasers for heterogeneous integration of optoelectronic integrated circuits, Photon. Integr. Photon. Electr. Convers. Silicon Platform 2 (2015) 45.
- [80] A.W. Fang, H. Park, O. Cohen, R. Jones, M.J. Paniccia, J.E. Bowers, Electrically pumped hybrid AlGaInAs-silicon evanescent laser, Opt. Express 14 (2006) 9203–9210.
- [81] A.W. Fang, E. Lively, Y.-H. Kuo, D. Liang, J.E. Bowers, A distributed feedback silicon evanescent laser, Opt. Express 16 (2008) 4413–4419.
- [82] B. Ben Bakir, A. Descos, N. Olivier, D. Bordel, P. Grosse, E. Augendre, L. Fulbert, J.M. Fedeli, Electrically driven hybrid Si/III-V Fabry-Pérot lasers based on adiabatic mode transformers, Opt. Express 19 (2011) 10317–10325.
- [83] S. Keyvaninia, G. Roelkens, D.V. Thourhout, C. Jany, M. Lamponi, A.L. Liepvre, F. Lelarge, D. Make, G.-H. Duan, D. Bordel, J.-M. Fedeli, Demonstration of a heterogeneously integrated III-V/SOI single wavelength tunable laser, Opt. Express 21 (2013) 3784–3792.
- [84] T. Creazzo, E. Marchena, S.B. Krasulick, P.K. Yu, D. Van Orden, J.Y. Spann, C.C. Blivin, L. He, H. Cai, J.M. Dallesasse, R.J. Stone, A. Mizrahi, Integrated tunable CMOS laser, Opt. Express 21 (2013) 28048–28053.
- [85] D. Liang, M. Fiorentino, S. Srivivasan, J.E. Bowers, R.G. Beausoleil, Low threshold electrically-pumped hybrid silicon microring lasers, IEEE J. Sel. Top. Quantum Electron 17 (2011) 1528–1533.
- [86] H.Z. Chen, A. Ghaffari, H. Wang, H. Morkoç, A. Yariv, Continuous-wave operation of extremely low-threshold GaAs/AlGaAs broad-area injection lasers on (100) Si substrates at room temperature, Optics Lett. 12 (10) (1987) 812–813.
- [87] M. Sugo, H. Mori, Y. Sakai, Y. Itoh, Stable cw operation at room temperature of a 1.5  $\mu$ m wavelength multiple quantum well laser on a Si substrate, Appl. Phys. Lett. 60 (4) (1992) 472–473.
- [88] M.E. Groenert, C.W. Leitz, A.J. Pitera, V. Yang, H. Lee, R.J. Ram, E.A. Fitzgerald, Monolithic integration of room-temperature cw GaAs/AlGaAs lasers on Si substrates via relaxed graded GeSi buffer layers, J. Appl. Phys. 93 (1) (2003) 362–367.
- [89] P. Petroff, R.L. Hartman, Defect structure introduced during operation of heterojunction GaAs lasers, Appl. Phys. Lett. 23 (1973) 469.
- [90] P.M. Petroff, R.L. Hartman, Rapid degradation phenomenon in heterojunction GaAlAs-GaAs lasers, J. Appl. Phys. 45 (1974) 3899–3903.
- [92] S. O'Hara, P.W. Hutchinson, P.S. Dobson, The origin of dislocation climb during laser operation, Appl. Phys. Lett. 30 (1977) 368.
- [93] O. Ueda, Degradation of III-V opto-electronic devices, J. Electrochem. Soc. 135 (1988) 11C.
- [94] Y. Hasegawa, T. Egawa, T. Jimbo, M. Umeno, Influences of dark line defects on characteristics of AlGaAs/GaAs quantum well lasers grown on Si substrates, Jpn. J. Appl. Phys. 34 (1995) 2994–2999.
- [95] O. Ueda, S.J. Pearton, Materials and Reliability Handbook for Semiconductor Optical and Electron Devices, Springer-Verlag, New York, NY, USA, 2013, pp. 90–96 p. 194.
- [96] L.C. Kimerling, Recombination enhanced defect reactions, Solid State Electr. 21 (1978) 1391–1401.
- [97] Z. Mi, J. Yang, P. Bhattacharya, G. Qin, and Z. Ma, High-performance quantum dot lasers and integrated optoelectronics on Si, Proc. IEEE 97(7) (2009) 1239–1249.
- [98] D. Lacombe, A. Ponchet, J.M. Gérard, O. Cabrol, Structural study of InAs quantum boxes grown by molecular beam epitaxy on a (001) GaAs-on-Si substrate, Appl. Phys. Lett. 70 (18) (1997) 2398–2400.
- [99] S. Chen, W. Li, J. Wu, Q. Jiang, M. Tang, S. Shutts, S.N. Elliott, A. Sobiesierski, A.J. Seeds, I. Ross, P.M. Smotrow, Electrically pumped continuous-wave III-V quantum dot lasers on silicon, Nat. Photonics 10 (2016) 307–311.
- [100] J. Yang, P. Bhattacharya, Z. Mi, High-performance  $In_{0.5}Ga_{0.5}$ As/GaAs quantum-dot lasers on silicon with multiple-layer quantum-dot dislocation filters, IEEE Trans. Electron. Devices 54 (2007) 2849–2855.
- [101] H. Liu, T. Wang, Q. Jiang, R. Hogg, F. Tutu, F. Pozzi, A. Seeds, Long-wavelength InAs/GaAs quantum-dot laser diode monolithically grown on Ge substrate, Nat. Photonics 5 (2011) 416–419 2011.
- [102] A.Y. Liu, C. Zhang, J. Norman, A. Snyder, D. Lubyshev, J.M. Fastenau, A.W. Liu, A.C. Gossard, J.E. Bowers, High performance continuous wave 1.3  $\mu$ m quantum dot lasers on silicon, Appl. Phys. Lett. 104 (4) (2014) 041104.
- [103] A.Y. Liu, R.W. Herrick, O. Ueda, P.M. Petroff, A.C. Gossard, J.E. Bowers, Reliability of InAs/GaAs quantum dot lasers epitaxially grown on silicon, IEEE J. Sel. Top. Quant. Electron 21 (6) (2015) 690–697.
- [104] A.Y. Liu, J. Peters, X. Huang, D. Jung, J. Norman, M.J. Lee, A.C. Gossard, J. Bowers, Electrically pumped continuous-wave 1.3  $\mu$ m quantum-dot lasers epitaxially grown on on-axis (001) GaP/Si, Optics Lett. 42 (2) (2017) 338–341.
- [105] J. Norman, M.J. Kennedy, J. Selvigne, Q. Li, Y. Wan, A.Y. Liu, P.G. Callahan, M.P. Echlin, T.M. Pollock, K.M. Lau, A.C. Gossard, J. Bowers, Electrically pumped continuous wave quantum dot lasers epitaxially grown on patterned, on-axis (001) Si, Opt. Express 25 (4) (2017) 3927–3934.
- [106] S. Chen, M. Liao, M. Tang, J. Wu, M. Martin, T. Baron, A. Seeds, H. Liu, Electrically pumped continuous-wave 1.3  $\mu$ m InAs/GaAs quantum dot lasers monolithically grown on on-axis Si (001) substrates, Opt. Express 25 (5) (2017) 4632–4639.
- [107] J. Bai, J.-S. Park, Z. Cheng, M. Curtin, B. Adekoré, M. Carroll, A. Lochtefeld, M. Dudley, Study of the defect elimination mechanisms in aspect ratio trapping Ge growth, Appl. Phys. Lett. 90 (10) (2007) 101902.
- [108] T.A. Langdo, C.W. Leitz, M.T. Currie, E.A. Fitzgerald, A. Lochtefeld, D.A. Antoniadis, High quality Ge on Si by epitaxial necking, Appl. Phys. Lett. 76 (2000) 3700.
- [109] B. Kunert, W. Guo, Y. Mols, B. Tian, Z. Wang, Y. Shi, D. Van Thourhout, M. Pantouvaki, J. Van Campenhout, R. Langer, K. Barla, III/V nano ridge structures for optical applications on patterned 300 mm silicon substrate, Appl. Phys. Lett. 109 (9) (2016) 091101.
- [110] J.Z. Li, J. Bai, J.-S. Park, B. Adekoré, K. Fox, M. Carroll, A. Lochtefeld, Z. Shellenbarger, Defect reduction of GaAs epitaxy on Si (001) using selective aspect ratio trapping, Appl. Phys. Lett. 91 (2007) 021114.
- [111] R. Cipro, T. Baron, M. Martin, J. Moeyaert, S. David, V. Gorbenko, F. Bassani, Y. Bogumiłowicz, J.P. Barnes, N. Rochat, V. Loup, Low defect InGaAs quantum well selectively grown by metal organic chemical vapor deposition on Si (100) 300 mm wafers for next generation non planar devices, Appl. Phys. Lett. 104 (2014) 262103.
- [112] W. Guo, L. Date, V. Pena, X. Bao, C. Merckling, N. Waldron, N. Collaert, M. Caymax, E. Sanchez, E. Vancoille, K. Barla, Selective metal-organic chemical vapor deposition growth of high quality GaAs on Si (001), Appl. Phys. Lett. 105 (2014) 062101.
- [113] T. Orzali, A. Vert, B. O'Brien, J.L. Herman, S. Vivekanand, R.J. Hill, Z. Karim, S.S. Papa Rao, GaAs on Si epitaxy by aspect ratio trapping: Analysis and reduction of defects propagating along the trench direction, J. Appl. Phys. 118 (2014) 105307.
- [114] C. Merckling, N. Waldron, S. Jiang, W. Guo, N. Collaert, M. Caymax, E. Vancoille, K. Barla, A. Thean, M. Heyns, W. Vandervorst, Heteroepitaxy of InP on Si (001) by selective-area metal organic vapor-phase epitaxy in sub-50 nm width trenches: The role of the nucleation layer and the recess engineering, J. Appl. Phys. 115 (2) (2014) 023710.
- [115] G. Wang, M.R. Leyls, R. Loo, O. Richard, H. Bender, N. Waldron, G. Brammertz, J. Dekoster, W. Wang, M. Seefeldt, M. Caymax, Selective area growth of high quality InP on Si (001) substrates, Appl. Phys. Lett. 97 (2010) 121913.
- [116] N. Waldron, G. Wang, N.D. Nguyen, T. Orzali, C. Merckling, G. Brammertz, P. Ong, G. Winderickx, G. Hellings, G. Eneman, M. Caymax, Integration of III-V on Si for high-mobility CMOS, Int. Silicon German. Technol. Device Meet. (2012).
- [117] J.Z. Li, J. Bai, J.M. Hydrick, J.G. Fiorenza, C. Major, M. Carroll, Z. Shellenbarger, A. Lochtefeld, Thin film InP epitaxy on Si (001) using selective aspect ratio trapping, ECS Trans. 18 (1) (2009) 887.
- [118] S. Li, X. Zhou, M. Li, X. Kong, J. Mi, M. Wang, W. Wang, J. Pan, Ridge InGaAs/InP multi-quantum-well selective growth in nanoscale trenches on Si (001) substrate, Appl. Phys. Lett. 108 (2016) 021902.
- [119] Y. Han, Q. Li, S.P. Chang, W.D. Hsu, K.M. Lau, Growing InGaAs quasi-quantum wires inside semi-rhombic shaped planar InP nanowires on exact (001) silicon, Appl. Phys. Lett. 108 (24) (2016) 242105.
- [120] Y. Han, Q. Li, K.M. Lau, Highly ordered horizontal indium gallium arsenide/indium phosphide multi-quantum-well in wire structure on (001) silicon substrates, J. Appl. Phys. 120 (24) (2016) 245701.
- [121] M. Paladugu, C. Merckling, R. Loo, O. Richard, H. Bender, J. Dekoster, W. Vandervorst, M. Caymax, M. Heyns, Site selective integration of III-V materials on Si for nanoscale logic and photonic devices, Cryst. Growth Des. 12 (10) (2012) 4696–4702.

- [122] P. Allongue, V. Costakieling, H. Gericke, Etching of Silicon in NaOH solutions, Etching of silicon in NaOH solutions: I . in situ scanning tunneling microscopic investigation of n-Si(111), *J. Electrochem. Soc.* 140 (1993) 1009.
- [123] J.-L. Lin, D.Y. Petrovskiy, J. Viernow, F.K. Men, D.J. Seo, F.J. Himpsel, Formation of regular step arrays on Si (111), *J. Appl. Phys.* 84 (1998) 255.
- [124] N. Waldron, C. Merckling, W. Guo, P. Ong, L. Teugels, S. Ansar, D. Tsvetanova, F. Sebaai, D.H. van Dorp, A. Milenin, D. Lin, An InGaAs/InP quantum well finfet using the replacement fin process integrated in an RMG flow on 300 mm Si substrates, *Symposium on VLSI Technology (VLSI-Technology)*, 2014.
- [125] N. Waldron, C. Merckling, L. Teugels, P. Ong, S.A.U. Ibrahim, F. Sebaai, A. Pourghaderi, K. Barla, N. Collaert, A.V.Y. Thean, InGaAs gate-all-around nanowire devices on 300 mm Si substrates, *IEEE Electron Device Lett.* 35 (11) (2014) 1097–1099.
- [126] Q. Li, Y. Han, X. Lu, K.M. Lau, GaAs-InGaAs-GaAs fin-array tunnel diodes on (001) Si substrates with room-temperature peak-to-valley current ratio of 5.4, *IEEE Electron Device Lett.* 37 (1) (2016) 24–27.
- [127] Y. Han, Q. Li, K.M. Lau, Monolithic integration of tunnel diode-based inverters on exact (001) Si substrates, *IEEE Electron Device Lett.* 37 (6) (2016) 717–720.
- [128] Y. Han, Q. Li, K.M. Lau, Fin-array tunneling trigger with tunable hysteresis on (001) silicon substrate, *IEEE Electron Device Lett.* 38 (5) (2017) 556.
- [129] T. Orzali, A. Vert, B. O'Brian, J.L. Herman, S. Vivekanand, S.S. Papa Rao, S.R. Oktyabrsky, Epitaxial growth of GaSb and InAs fins on 300 mm Si (001) by aspect ratio trapping, *J. Appl. Phys.* 120 (8) (2016) 085308.
- [130] Z. Wang, B. Tian, M. Paladugu, M. Pantouvaki, N. Le Thomas, C. Merckling, W. Guo, J. Dekoster, J. Van Campenhout, P. Absil, D. Van Thourhout, Polytypic InP nanolaser monolithically integrated on (001) silicon, *Nano Lett.* 13 (11) (2013) 5063–5069.
- [131] Z. Wang, B. Tian, M. Pantouvaki, W. Guo, P. Absil, J. Van Campenhout, C. Merckling, D. Van Thourhout, Room-temperature InP distributed feedback laser array directly grown on silicon, *Nat. Photonics* 9 (12) (2015) 837–842.
- [132] L. Czornomaz, E. Uccelli, M. Sousa, V. Deshpande, V. Djara, D. Caimi, M.D. Rossell, R. Erni, J. Pompeyrene, Confined epitaxial lateral overgrowth (CELO): a novel concept for scalable integration of CMOS-compatible InGaAs-on-insulator MOSFETs on large-area Si substrates, *Symposium on VLSI Technology*, 2015, pp. T172–T173.
- [133] Z. Wang, C. Junesand, W. Metaferia, C. Hu, L. Wosinski, S. Lourdudoss, III-Vs on Si for photonic applications—a monolithic approach, *Mater. Sci. Eng.* 177 (17) (2012) 1551–1557.
- [134] H. Kataria, W. Metaferia, C. Junesand, C. Zhang, N. Julian, J.E. Bowers, S. Lourdudoss, Simple epitaxial lateral overgrowth process as a strategy for photonic integration on silicon, *IEEE J. Sel. Top. Quant. Electron.* 20 (2014) 8201407.
- [135] J.G. Fiorenza, J.S. Park, J. Hydrick, J. Li, J.Z. Li, M. Curtin, M. Carroll, A. Lochtefeld, Aspect ratio trapping: a unique technology for integrating Ge and III-Vs with silicon CMOS, *ECS Trans.* 33 (6) (2010) 963–976.
- [136] J.Z. Li, J. Bai, C. Major, M. Carroll, A. Lochtefeld, Z. Shellenbarger, Defect reduction of GaAs/Si epitaxy by aspect ratio trapping, *J. Appl. Phys.* 103 (2008) 106102.
- [137] Y.Q. Wu, M. Xu, P.D. Ye, Z. Cheng, J. Li, J.S. Park, J. Hydrick, J. Bai, M. Carroll, J.G. Fiorenza, A. Lochtefeld, Atomic-layer-deposited Al<sub>2</sub>O<sub>3</sub>/GaAs metal-oxide-semiconductor field-effect transistor on Si substrate using aspect ratio trapping technique, *Appl. Phys. Lett.* 93 (24) (2008) 242106.
- [138] S.L. Rommel, D. Pawlik, P. Thomas, M. Barth, K. Johnson, S.K. Kurinec, A. Seabaugh, Z. Cheng, J.Z. Li, J.S. Park, J.M. Hydrick, Record PVCR GaAs-based tunnel diodes fabricated on Si substrates using aspect ratio trapping, *IEEE Int. Electron Devices Meet.* (2008).
- [139] Q. Li, K.W. Ng, K.M. Lau, Growing antiphase-domain-free GaAs thin films out of highly ordered planar nanowire arrays on exact (001) silicon, *Appl. Phys. Lett.* 106 (2015) 072105.
- [140] Y. Wan, Q. Li, Y. Geng, B. Shi, K.M. Lau, InAs/GaAs quantum dots on GaAs-on-V-grooved-Si substrate with high optical quality in the 1.3 μm band, *Appl. Phys. Lett.* 107 (8) (2015) 081106.
- [141] Y. Wan, Q. Li, A.Y. Liu, A.C. Gossard, J.E. Bowers, J.E. Hu, K.M. Lau, Optically pumped 1.3 μm room-temperature InAs quantum-dot micro-disk lasers directly grown on (001) silicon, *Optics Lett.* 41 (7) (2016) 1664–1667.
- [142] Y. Wan, Q. Li, A.Y. Liu, W.W. Chow, A.C. Gossard, J.E. Bowers, E.L. Hu, K.M. Lau, Sub-wavelength InAs quantum dot micro-disk lasers epitaxially grown on exact Si (001) substrates, *Appl. Phys. Lett.* 108 (22) (2016) 221101.
- [143] Q. Li, Y. Wan, A.Y. Liu, A.C. Gossard, J.E. Bowers, E.L. Hu, K.M. Lau, 1.3-μm InAs quantum-dot micro-disk lasers on V-groove patterned and unpatterned (001) silicon, *Optics Express* 24 (18) (2016) 21038–21045.



**Qiang Li** is currently a research assistant professor with the Department of Electronic and Computer Engineering, Hong Kong University of Science and Technology (HKUST). He received his B.S. degree in microelectronics from Peking University in 2009 and Ph.D. in electronic and computer engineering from HKUST in 2014. His present research focuses on lattice-mismatched epitaxy of III-V compound semiconductors on silicon for electronic-photonics heterogeneous integration.



**Kei May Lau** is Fang Professor of Engineering at the Hong Kong University of Science and Technology (HKUST). She received the B.S. and M.S. degrees in physics from the University of Minnesota, Minneapolis, and the Ph.D. degree in Electrical Engineering from Rice University, Houston, Texas. She was on the ECE faculty at the University of Massachusetts/Amherst and initiated MOCVD, compound semiconductor materials and devices programs. Since the fall of 2000, she has been with the ECE Department at HKUST. She established the Photonics Technology Center for R&D effort in III-V materials, optoelectronic, high power, and high-speed devices. Professor Lau is a Fellow of the IEEE, and a recipient of the US National Science Foundation (NSF) Faculty Awards for Women (FAW) Scientists and Engineers (1991), Hong Kong Croucher Senior Research Fellowship (2008) and IEEE Photonics Society Aron Kressel Award (2017). She is an Editor of the IEEE EDL and Associate Editor of Applied Physics Letters.